Prognostic Precipitation in the Lokal Modell (LM) of the German Weather Service

Michael Baldauf[1], German Weather Service

Introduction

In the current operational version of the Lokal Modell (LM) of the German Weather Service (Doms and Schättler, 2002) the conservation equations for rain and snow

$$\rho \frac{\partial q^x}{\partial t} + \rho \mathbf{v} \cdot \nabla q^x = -\nabla \cdot \mathbf{P}^x - \nabla \cdot \mathbf{F}^x + S^x \tag{1}$$

($x = r, s$ for rain, snow, q= mixing ratio, $\mathbf{P}$= sedimentation flux, $\mathbf{F}$= turbulent flux, S= source terms from cloud microphysics) are approximated stationary and without advection. This column equilibrium approach means that precipitation particles, arising from cloud microphysical processes, immediately fall down to the bottom in the same time step. Rain drops with a mean fall velocity of about 5 m/s which develop for example in a height of 3 km, need a falling time of 10 min. and then are drifted 6 km (by an assumed horizontal wind of 10 m/s). For snow with a mean fall velocity of about 1 m/s (and usually generated higher up) the horizontal drift is even larger. Therefore, for the LM with a grid length of currently 7 km (in the next version (LMK) a grid length of about 2.8 km is aspired) and a time step of 40 sec. the column equilibrium approach is no longer valid. This was inspected by case studies especially to the luff-lee-problem: in many models precipitation falls to much on the upwind side of mountains, whereas the measured precipitation maximum even often lies in the lee. Especially for hydrologists the solution of this luff-lee-problem is of relevance: precipitation flows in the false valleys and therefore is added to a false waters catchment area.

Semi-Lagrange-Advection

There are in principal two possibilities to handle the sedimentation term $-\partial P_z/\partial z$: either this term is discretized directly (for example implicit) or one writes the sedimentation flux as a product of an effective fall velocity and the density $P_z = v_{eff} \rho q$ and handles it in the advection scheme. In the last case one has to consider, that in LM the near to the ground layers are so thin (about 60 m), that with the currently used time step of 40 sec., particles can fall through up to three thickness layers per time step. Therefore one needs an advection scheme which remains stable up to vertical Courant numbers of about 3. Apart from this, the prognostic precipitation shall be implemented in the version LMK, in which horizontal Courant numbers up to 1.8 are aspired, for that most Eulerian advection schemes are no longer stable. For the advection of precipitation we therefore decided to use a threedimensional Semi-Lagrange (SL) scheme (e.g. Staniforth and Côté, 1991) whose stability does not depend on the Courant number.

The application of the standard SL schemes consists of two steps: 1. calculation of the backtrajectory and 2. interpolation of the fields q^r and q^s at the starting point. The implicit equation of the backtrajectory (Robert, 1981) is solved by iteration; after one iteration step one gets a truncation error of order $O(\Delta t)$, after two steps an order $O(\Delta t^2)$. Simple tests show, that an error of only $O(\Delta t)$ delivers especially nonsatisfying conservation properties; this is in agreement with Staniforth and Côté (1991), who also recommend an order $O(\Delta t^2)$. The therefore needed second iteration step requires an interpolation of the three velocity components. This interpolation is a time consuming step in the staggered Arakawa-C-grid; currently it needs more then 80 percent of the calculation time of the whole SL-scheme.

In the second interpolation step for the fields often a cubic polynomial is recommended, which shows the best relation between calculation amount and accuracy; especially the cubic spline interpolation is even ideally conserving. In contrast, for the time being we use the more simple and computer time saving trilinear (i.e. linear in all three space dimensions) interpolation. It is well known that it has bad form properties (high diffusion) and only moderate conservation properties. However, the latter is probably not significant for rain and snow which remains only a few time steps in the model area. A test with a Gaussian rain particle distribution, which is advected with a given velocity ($u = 10$ m/s and $w = -5$ m/s), yielded a mass loss of 0.05 percent per time step. After 15 time steps (according to the example above) the mass loss is less then 1 percent. Similar tests with a velocity field over mountains even yielded a small gain of mass. But this could be connected with a non divergence free velocity field; in this case the advection itself does not conserve mass.

[1] Michael.Baldauf@dwd.de; Deutscher Wetterdienst, Kaiserleistr. 42, D-63067 Offenbach

A certain diffusion of the linear interpolation is even desired, as well, and could cure the problem of an unrealistic strong small scale structure of the precipitation in irregular terrain. Another advantage of the trilinear interpolation in contrast to higher order interpolation is its positive definiteness; an essential condition for the coupling to the cloud microphysics.

Coupling with cloud microphysics and real test cases

The dynamic core of the current operational LM consists of a 3-timelevel-scheme with time splitting by Klemp und Wilhelmson (1978). In the frame of this dynamic core the coupling between advection and cloud physics is done with a Marchuk-splitting, this means that in one time step the SL-advection from timelevel t^{n-1} to t^{n+1} (with velocities at t^n) is calculated and then with the updated values the cloud physics scheme is carried out. The latter is formulated implicitly, as mentioned above, but can be solved quasi-explicitly, because the sedimentation velocity is always directed downwards and therefore the system of equations has diagonal form.

The figures below show the whole precipitation (rain + snow) during a 24 h period for 20.02.2002+6-30 h over Southwest-Germany. The left figure shows a simulation with the operational LM, the right the same situation with the new prognostic precipitation scheme. The spatial precipitation distribution in the new scheme is much more similar to the observations (middle figure) than the current LM: the maxima are reduced (the operational LM overestimated them up to 150 %, the new version only by 20 %), the maxima are shifted to the lee side and therefore the unrealistic dry regions in the lee do not arize. The measured precipitation distribution had a mean value of about 16 kg/m^2, the operational LM-version yielded 30 % too much, the new version about 10 % too much. The calculation amount for the new version is about 20 % higher than the operational version, which seems acceptable for two new prognostic variables (q_r and q_s).

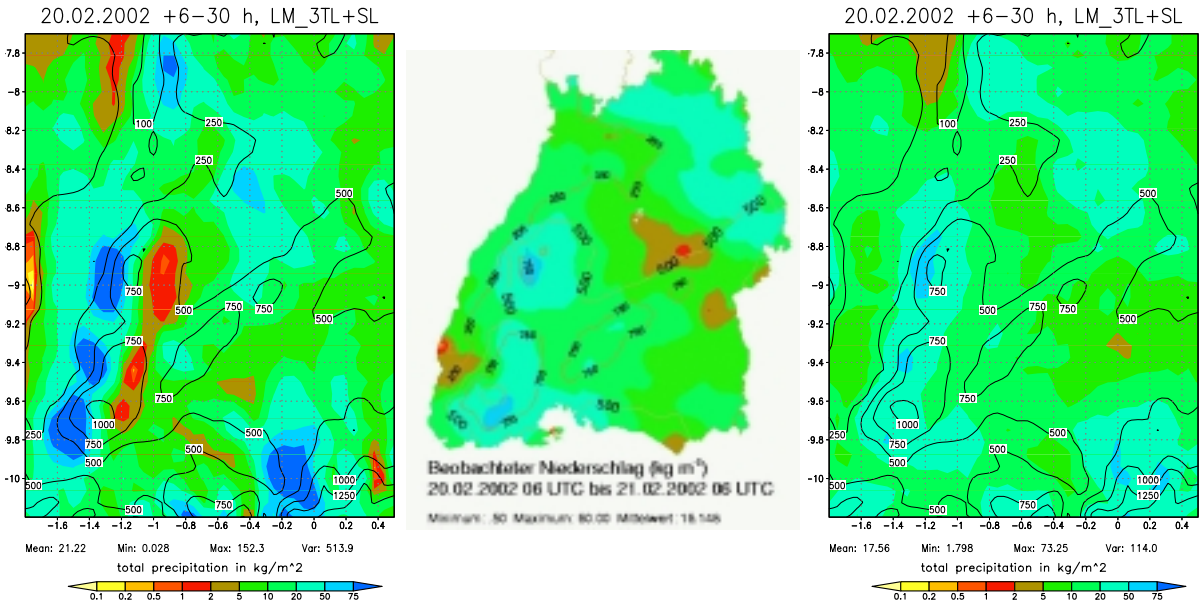

Figure 1: Simulation of the day 20.02.2002+6-30 h with the current operational LM without (left) and with (right) prognostic precipitation; observations (middle).

References

Staniforth, A. and Côté, J. (1991): Semi-Lagrangian Integration Schemes for Atmospheric Models - A Review, Mon. Wea. Rev., 119, 2206-2223.

Robert, A. (1981): A stable numerical integration scheme for the primitive meteorological equations, Atmos. Ocean, 19, 35-46.

Klemp, J. B. and Wilhelmson, R. B. (1978): The simulation of three-dimensional convective storm dynamics, J. Atmos. Sci., 35, 1070-1096

Doms, G. and Schättler, U. (2002): A description of the Nonhydrostatic Regional Model LM, http://cosmo-model.cscs.ch/cosmoPublic/

Development of a NWP System for Very Short-Range Forecasts

Günther Doms and Jochen Förstner
Deutscher Wetterdienst, P.O.Box 100465, 63004 Offenbach a.M., Germany
e-mail: guenther.doms@dwd.de, jochen.foerstner@dwd.de

For very detailed short range forecasts, the Deutscher Wetterdienst (DWD) has started the development of a meso-γ version of the operational nonhydrostatic regional model LM. This new version, called LMK, will utilize a grid-spacing of 2-3 km with about 50 vertical layers and an integration domain of about 1300 x 1300 km^2 (see Fig.1). LMK is aiming at the explicit prediction of deep convection and will provide 18-h forecasts for Germany eight times per day based on all observations available, including satellite and radar data. The development work is organized by an internal 3-years project from end 2003 to end 2006, with the operational implementation of the LMK system scheduled for late 2006.

With the new system, it is intended to fill the gap between traditional nowcasting methods for severe weather events (up to 3-6 hrs) and current short-range NWP with grid spacings of about 10 km and forecast ranges up to 48-72 hrs. In the time range of 18 hrs severe weather often forms in context with deep moist convection (such as super- and multi-cell thunderstorms, squall-lines, mesoscale convective complexes and mesocyclones) or due to interactions with fine-scale topography (such as fog, severe downslope winds, Föhn-storms, flash-floodings, etc.). As these events cannot be resolved with the resolution of present models, their prediction is in general very poor. However, there is a strong public demand for improved weather forecasts at finer scales and shorter ranges. An accurate prediction of extreme rainfall events or severe wind gusts in both time and space is especially required for hydrological, civil protection and environmental agencies to issue adequate warnings.

We expect a number of potential benefits of running a forecasts model routinely with a grid spacing better than 3 km on a quite large domain (to keep some internal predictability), since many more mesoscale weather systems and their scale interactions including local topographical effects can be properly resolved. Such a resolution will allow to simulate deep convective clouds directly and many deficiencies introduced by parameterized convection are removed. This means that the life-cycle of individual clouds can be represented in detail together with dynamic interactions and organization, resulting in features like supercell and squall-line formation or storm-cell initiation by gust fronts. It is expected that this will allow for much more realistic and hopefully more accurate forecasts of severe weather events. Deriving the convective-scale LMK from the LM requires a not only an adjustment of the existing schemes but also a development of new components within data assimilation, dynamics and numerics, physical parameterization, verification and validation. The project structure is organized along these points.

With respect to numerics, current work focuses on the the implementation of a TVD-variant of the 3rd-order in time Runge-Kutta time integration. The scheme can easily be combined with the standard time-split forward-backward methods to integrate fast compression waves and furthermore allows for flexible use of high-order spatial advection operators. From the latter, we expect noticeable benefits for simulating processes such as deep convective cloud evolution which is at or close to the grid-scale. Using a 5th-order advection scheme, the new scheme allows for a time step almost twice as large as with the standard Leapfrog/2nd-order centered differencing scheme of LM. This advantage is somewhat reduced since the advection operator has to be calculated three times. The main reason for applying the new time scheme, however, is not to save CPU-time but to achieve a more accurate and thus much better converged numerical solution at neutral computational costs. For first results from the RK3 time integration see the paper by Förstner and Doms in this volume.

The equations for the hydrological cycle have also to be reconsidered for very high spatial resolution, since advective transport of precipitation particles (like rain and snow) may no longer be neglected as it is done in current schemes. Hence, the present diagnostic treatment of precipitation has to be replaced by an algorithm based on the full 3-d budget equations for rain and snow. For LMK, a numerical algorithm to solve these prognostic equations has been constructed by combining a 3-d semi-Lagrangian advection scheme with an implicit treatment of precipitation fallout (see paper by Baldauf, this volume). Tests of the scheme indicate that the horizontal transport of snow is essential for correcting an erroneous

spatial distribution of precipitation of orographically forced rainfall in case of stable stratification. In case of high-resolution applications, the vertical advective transport of precipitation will be of crucial importance for describing the life-cycle of deep convective storms correctly.

Considering physical processes on the meso-γ scale, parameterization issues related to deep convection and gravity waved drag will disappear due to a direct simulation of these processes. Shallow convection, however, will still remain sub-grid scale and can play a significant role for initiating deep convection. At present, it is not clear if standard global-scale convection schemes based on steady-state plume cloud models with a moisture- or moist static energy convergence closure can cope with shallow convection at very high resolution. We plan to develop a shallow-convection scheme based on a dynamic cloud model, which allows for an explicit calculation of entrainment and detrainment, and a closure based on PBL turbulent kinetic energy. Remaining parameterized physical processes are turbulent mixing, microphysics, radiation and surface fluxes. For the latter two, we initially rely on the standard parameterization used in LM. Turbulent transport becomes essentially 3-d at very high resolution, e.g. lateral exchange across cloud boundaries will be important for the evolution and organization of deep convection. A new 3-d turbulence scheme based on turbulent kinetic energy using a non-isotropic closure for fluxes has been developed and is currently implemented. A more comprehensive treatment of the ice-phase is also important when simulating deep clouds directly. In this aspect, we will upgrade the present microphysics scheme to include graupel (and later on hail) as an additional precipitation category.

It is planned to run the LMK every 3 hours from a continuous data assimilation stream based on the LM observational nudging technique (Fig.1). Such a rapid update cycle will require a short data cut-off (less than 30 min) and the successful use of available non-synoptic remote sensing data. In this respect, the assimilation of radar reflectivities using the latent heat nudging (LHN) technique is under evaluation and satellite data will be assimilated by using profiles obtained with 1-D var retrievals. The LHN will be based on 5-min reflectivities, which requires the development of corresponding data correction algorithms and data quality control methods as well as the development of a European composite.

Verification and validation of high-resolution model forecasts is very difficult as representativity errors, spatial and temporal variability, and lack of suitable data become important - resulting in a less meaningful applicability of traditional quantitative scores. In the LMK project, we will focus on the use of a radar simulation model (to compare directly with radar measurements) and pseudo satellite imaginary in various channels, combined with new verification tools such as pattern recognition methods. These activities go along with the development of appropriate diagnostic tools and derivation of necessary products for customers.

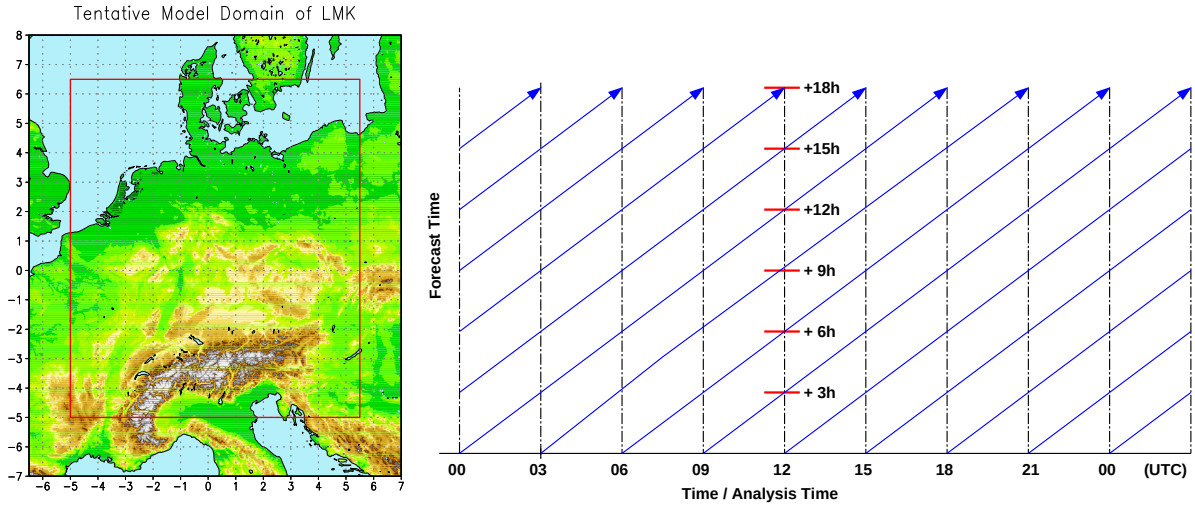

Figure 1: Tentative integration domain for LMK (left) and planned update cycle with forecasts every 3 hours (right). At a given time, 6 forecasts are available, allowing to generate some lagged averaging ensemble products.

IMPACT OF MODEL ERROR AND IMPERFECT INITIAL CONDITION PERTURBATIONS ON ENSEMBLE-BASED PROBABILISTIC FORECASTS: UNPREDICTABLE SPOTS

Jun Du*

SAIC at Environmental Modeling Center/NCEP/NOAA, Washington DC, U.S.A.

Given existing of intrinsic uncertainties in both initial condition (IC) and model (physics and dynamics), ensemble approach is the way to possibly give a full picture of future state of atmosphere. The ultimate goal of ensemble forecasting is to reliably estimate the time-evolution of probabilistic density function (PDF) of meteorological fields. However, due to model error and imperfect IC perturbations used in real-world ensemble prediction systems (EPS), it is believed that this task is extremely difficult if not impossible. Currently, little is known about the impact of model error or imperfect IC perturbations on the evolution of ensemble-based PDF in operational numerical weather prediction (NWP) models.

In this study, using the NCEP short-range ensemble forecasting (SREF) system (Du et. al. 2004, http://wwwt.emc.ncep.noaa.gov/mmb/SREF/SREF.html), the following three issues will be discussed: (1) given a near-perfect EPS, how well PDF can be predicted? (2) how to identify "bad" PDF forecast regions [defining as *"unpredictable spots"* (see the context below)] so that a special post processing might be applied to these regions? and (3) what is the relative importance between model error and imperfect IC perturbations over PDF evolution? Since there is no way to know "true" PDFs in real atmosphere, two "perfect model" experiments were conducted to study these issues.

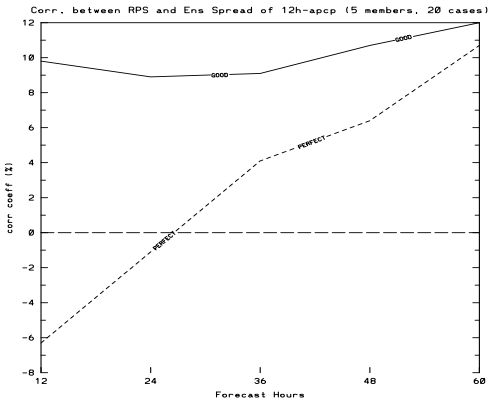

Figure 2: Spatial correlation between RPS score and ensemble spread for near *"perfect"* (dash) and *"good"* (solid) EPS, averaged over 20 cases during August and September 2003.

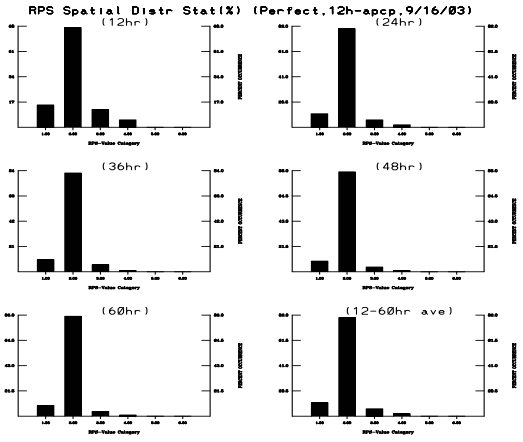

Figure 1: Percentage distribution of grid points over six RPS score categories for 12h, 24h, 36h, 48h and 60h probability forecasts as well as 12-60h average. It is from the near *perfect* EPS using 09z, Sept. 16, 2003 case as an illustration.

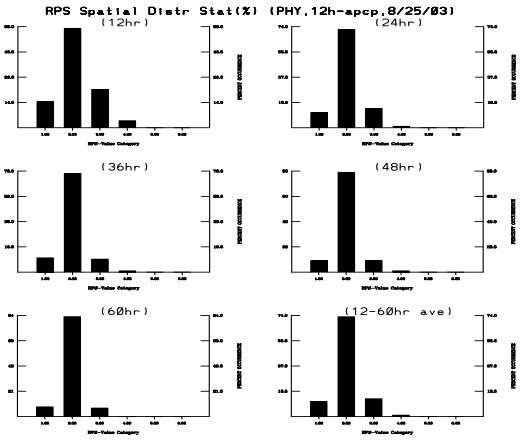

Figure 3: Same as Fig. 2 but for "perfect IC perturbation but slight model error" scenario (Eta.KF) using 21z, Aug. 25, 2003 case as an example.

* *Corresponding author address:* Dr. Jun Du, Environmental Modeling Center/NCEP, 5200 Auth Road, Camp Springs, MD 20746, USA; e-mail <Jun.Du@noaa.gov>

EPS	membership	model/physics	IC/perturbations	representativeness
Eta.BMJ	5	Eta with BMJ convective scheme	EDAS/bred from Eta.BMJ	*"truth"*
RSM.SAS	5	RSM with SAS convective scheme	GDAS/bred from RSM.SAS	very *"good"* system
Eta.KF	5	Eta with KF convective scheme	EDAS/bred from Eta.KF	near *"perfect"* system

Table 1: Design of Experiment I: how well PDF can be predicted with a near perfect EPS?

category	1	2	3	4	5	6
RPS value	0	(0,1)	[1,2)	[2,3)	[3,4)	4
meaning	perfect	good	useful	bad	worse	worst

Table 2: Definition of RPS score category. For a probability distribution over 5 MECE categories, the perfect RPS score is 0.0 and the worst is 4.0 (completely opposite).

Table 1 describes the design of Experiment I. Since it's reasonable to assume that the difference between current NWP models (analyses) and real atmospheric system (state) is much bigger than that between any two "good" operational NWP models (analyses), the EPS of Eta.KF could represent a near *"perfect"* system, while the "RSM.SAS" a very *"good"* system with respect to the *"true"* system (Eta.BMJ). Given such ideal EPSs, how well PDF could be predicted?

For simplicity as well as its importance, only 12h accumulated precipitation (12h-apcp) field was investigated as an example. For both *"good"* and *"perfect"* EPSs, their general performances (domain-averaged scores), as expected, are reasonably good in all aspects including ensemble mean, spread and probability distribution verifying against the *"truth"* (not shown).

Although the domain-wise performance is reasonably good, what is spatial variation of the performance? Figure 1 shows the percentage distribution of grid points over six RPS score categories (Table 2) from the near *"perfect"* EPS. Although majority of grid points (about 90 %) have good probability forecast (category 1 and 2), about 1 % of grid points have extremely bad probability forecast (categories 4 and 5) averaged over 20 cases during August and September 2003. For the *"good"* EPS, the number of grid points having "bad" probability forecast increased to about 2 % with a small number of grid points even entering category 6! (not shown). Further study shows that over these "bad-PDF" regions, not only probability forecast is bad, but ensemble spread and mean forecasts are all bad (not shown). These "bad PDF" spots can be defined as **"unpredictable spots"** since even a near-perfect EPS cannot predict it well over those spots.

One can imagine that almost any of current statistical post-processing methods (bias, spread, PDF corrections) to an EPS is based on general performance (statistics) of past forecasts, therefore, won't help to correct a future forecast over those "unpredictable spots" where calibration is really needed the most. Since "unpredictable spots" changes in location and time from case to case, **a location and time dependent post-processing method is strongly desired!**

A big question is that is it possible and how to identify those "unpredictable spots" *in prior*?. Is it possible that those "unpredictable spots" are associated with highly unpredictable regions where ensemble spread is large? Unfortunately, the answer is NO. Figure 2 shows that "unpredictable spots" are not closely correlated to ensemble spread. Therefore, it's very difficult if not impossible to locate those spots.

Table 3 (removed due to page limit) is the design of experiment II. 9 cases from August 2003 were investigated. Results are shown in Fig. 3 (model error only) and Fig 4 (imperfect IC perturbation only, removed due to page limit). Figure 3 tells us that **as long as model error exists (always the case in real world), it is almost certain that there are some spots which cannot be predicted even given a perfect IC perturbation distribution!** Figure 4 implies that only if given a perfect model plus a very realistic IC perturbations (Eta.BMJx), good probability forecast at all locations becomes a possibility although it's still not a perfect forecast (majority enter category 2 and a small number of points still enter category 3 which is not a good but useful forecast). This result vividly illustrates that how tough the task is to predict PDF correctly based on ensemble in operational environment!

References

Du, J., J. McQueen, G. DiMego, T. Black, H, Juang, E. Rogers, B. Ferrier, B. Zhou, Z. Toth and M. S, Tracton, 2004: The NOAA/NWS/NCEP short-range ensemble forecast (SREF) system: evaluation of an initial condition vs multi-model physics ensemble approach. Preprints (CD), 16th Conference on Numerical Weather Prediction, Seattle, Washington, Amer. Meteor. Soc.

A HIGH-RESOLUTION WIDE-RANGE NUMERICAL SIMULATION OF CLOUD BANDS ASSOCIATED WITH THE JAPAN SEA POLAR-AIR MASS CONVERGENCE ZONE IN WINTER USING A NON-HYDROSTATIC MODEL ON THE EARTH SIMULATOR

Hisaki Eito, Chiashi Muroi, Syugo Hayashi, Teruyuki Kato and Masanori Yoshizaki

Meteorological Research Institute, Japan Meteorological Agency, Tsukuba, Japan

1. INTRODUCTION

During winter monsoon season, broad cloud bands extending southeastward from the base of the Korean Peninsula sometimes bring heavy snowfalls to the Sea of Japan-side coastal regions of Japan Islands. These cloud bands form over the low-level convergence zone (Japan Sea Polar-air mass Convergence Zone; JPCZ) between two cold airflows with different property. In this study, a high-resolution wide-range simulation of cloud bands associated with the JPCZ is performed using a non-hydrostatic model (NHM) with 1-km horizontal resolution and 2000 x 2000 km calculation domain on the Earth Simulator (ES). The case studied is a typical broad cloud bands that developed over the Sea of Japan on 14 January 2001.

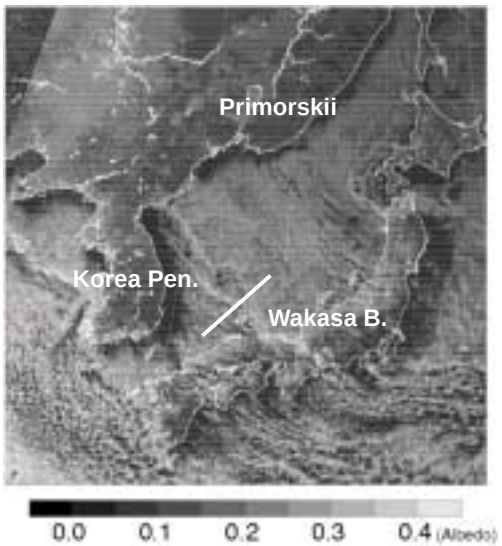

Fig. 1: GMS-5 visible imagery at 14 JST on 14 January 2001. A white solid line shows the flight path of an instrumental aircraft.

2. OBSERVATIONS

Figure 1 shows the GMS-5 visible imagery at 14 JST on 14 January 2001. Several clouds were found over the Sea of Japan, as a consequence of heat and moisture supply to continental cold air mass. The remarkable cloud bands, where cumulus convections developed, were distributed over the Sea of Japan from the base of the Korean Peninsula to Wakasa Bay. These cloud bands were also observed with an instrumental aircraft (Murakami et al., 2002). The conceptual model of the cloud bands, which is derived on a basis of the aircraft observation, is shown in Fig. 2. Air-mass on the SW side of JPCZ was warmer. Longitudinal mode (L-mode) cloud streets with top height of ~3 km observed in the SW side of JPCZ were taller than those in the NE side (~2 km). Deepest (~4 km) convective clouds formed on the southwestern edge of the JPCZ. Transverse mode (T-mode) clouds were mainly produced by anvil clouds (ice and snow particles) blowing from the deepest convective clouds.

Corresponding author address: Hisaki Eito,
Meteorological Research Institute,
Japan Meteorological Agency,
Nagamine, Tsukuba, Ibaraki 305-0052, Japan,
E-mail: heito@mri-jma.go.jp

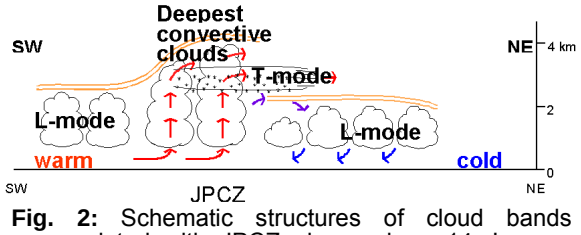

Fig. 2: Schematic structures of cloud bands associated with JPCZ observed on 14 January 2001 (from Murakami et al., 2002).

3. NUMERICAL MODELS

The NHM developed by Japan Meteorological Agency (JMA) is used in this study (Saito et al., 2001, JMA-NHM). The fully compressible equations with the conformal mapping are employed as the basic equations of JMA-NHM. Primary physical processes such as cloud physics, atmospheric radiation and mixing in the planetary boundary layer are also included in JMA-NHM. The JMA-NHM has been transferred to the ES, which is the fastest supercomputer in the world. In the present study, the JMA-NHM has a horizontal grid size of 1km with 2000 x 2000 grid points (1km-NHM). The vertical grid with a terrain-following coordinate contains 38 levels with a variable grid interval of 40 m near the surface and 1090 m at the top of the domain. The model top is 20.36 km. The time step interval is 5 seconds. The 1km-NHM is one-way nested within the JMA-NHM with a 5-km grid forecast (5km-NHM). The initial and boundary conditions for the 5km-NHM are provided from output produced by Regional Spectral Model (RSM). The RSM with a horizontal grid size of about 20km is a hydrostatic model used operationally in JMA.

4. RESULTS

The 1km-NHM successfully reproduced cloud bands associated with the JPCZ extending southeastward from the base of the Korean Peninsula to the San-in and Hokuriku district over the Sea of Japan (Fig. 3). Several cloud streets were also calculated around cloud bands. The 5km-NHM also well reproduced the features of cloud bands and other clouds (Fig. 4). However, more detailed features were not reproduced by the 5km-NHM. Figure 5 shows the structures of cloud bands in a vertical cross section on the white line in Fig. 3. The JPCZ formed between warmer west-northwesterly and colder north-northwesterly flows in the lower level. A strong horizontal convergence line was situated at the southwestern edge of the JPCZ. Deep convective clouds with the height of ~4 km formed along the line. L-mode cloud streets with top height of ~3 km were calculated on the SW side of the JPCZ. The top height of L-mode cloud streets calculated on the NE side of the JPCZ was lower (~2 km). These features almost agreed with those of the aircraft observation. However, effects of anvil-like snow and ice particles were small in the model-simulated T-mode clouds. Model-simulated T-mode clouds looked like developed convective clouds. Satellite and radar observations indicate that both convective and anvil-like clouds were responsible for the origin of T-mode clouds.

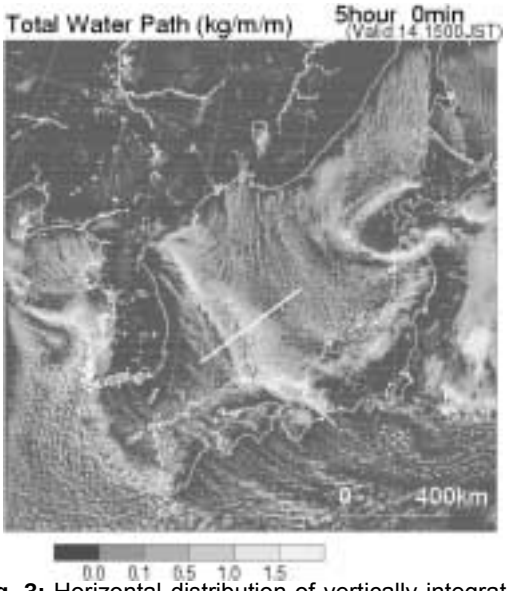

Fig. 3: Horizontal distribution of vertically integrated condensed water simulated by the 1km-NHM.

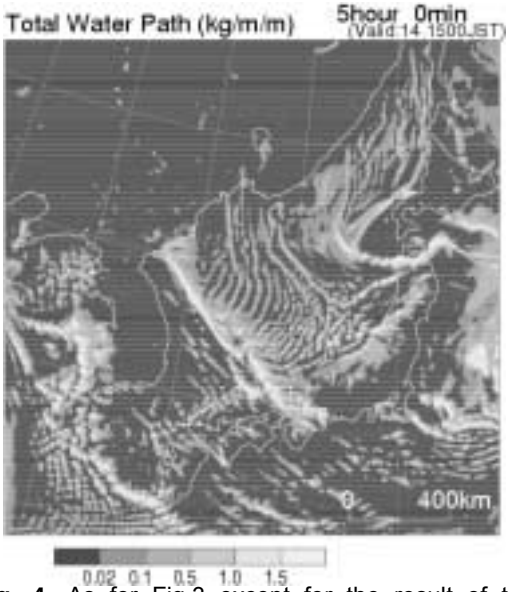

Fig. 4: As for Fig.3 except for the result of the 5km-NHM.

5. SUMMARY

A high-resolution wide-range numerical simulation of cloud bands associated with the JPCZ was performed using a NHM on the ES with 1-km horizontal resolution and 2000 x 2000 km calculation domain. Cloud features observed by a meteorological satellite were well reproduced in the model. Detailed structures of the cloud bands associated with the JPCZ were almost corresponded with those by in-situ airplane observations except for the aspect of T-mode clouds. It is necessary to examine the process of cloud microphysics in the model and also to carry out the comparison with the other cases.

Acknowledgements

This study is conducted by the fund of Research Revolution 2002, and the numerical calculations are made by NEC SX-6 on Earth Simulator.

References

Murakami M., M. Hoshimoto, N., Orikasa, H. Horie, H. Okamoto, H. Kuroiwa, H. Minda and K. Nakamura, 2002: Inner structures of snow bands associated with the Japan Sea Polar-airmass Convergence Zone based on aircraft observations. *Proc. International conference on mesoscale convective systems and heavy rainfall/snowfall in East Asia*, 522-527.

Saito, K., T. Kato, H. Eito and C. Muroi, 2001: Documentation of the Meteorological Research Institute/ Numerical Prediction Division Unified Nonhydrostatic Model. *Tec. Rep. MRI*, **42**, 133 pp.

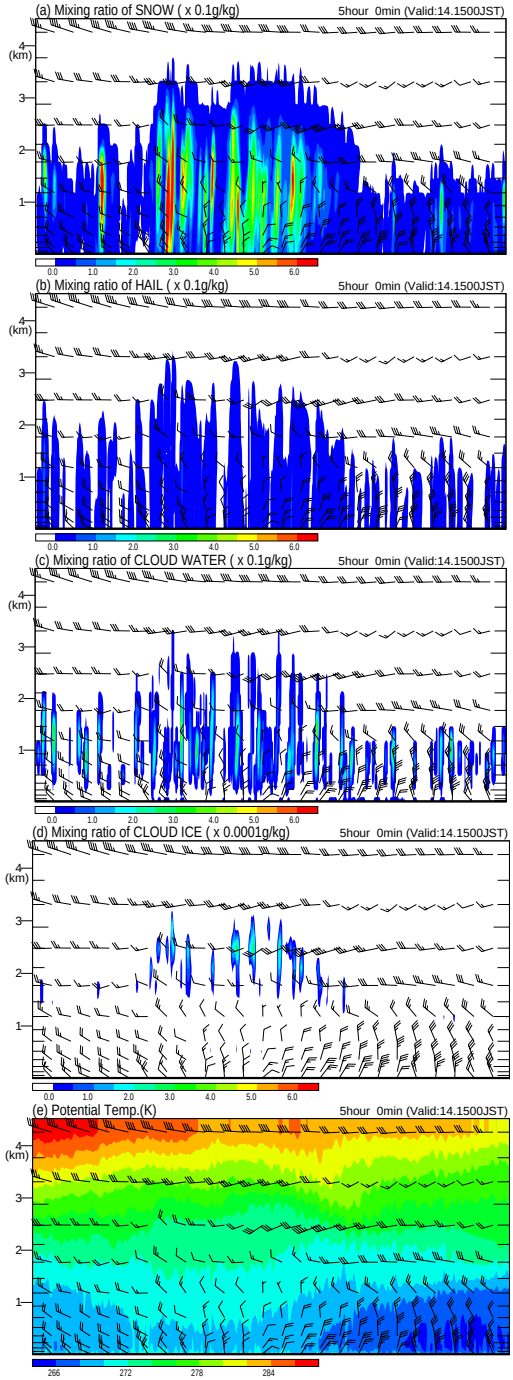

Fig. 5: Structures of cloud bands in a vertical cross section on the white solid line in Fig. 3. (a) Mixing ratio of snow. (b) Mixing ratio of graupel. (c) Mixing ratio of cloud water. (d) Mixing ratio of cloud ice. (e) Potential temperature. Barbs denote horizontal wind velocity at each level.

Simulations of warm season MCS rainfall using mixed physics in the Eta and WRF models

William A. Gallus, Jr. and Isidora Jankov
Dept. of Geological and Atmospheric Science, Iowa State University, Ames, IA
email: wgallus@iastate.edu

Warm season mesoscale convective systems (MCSs) have been simulated over the Central United States in two regional domains to determine if any particular combination of model physics consistently produces the best rainfall forecast. All model runs were integrated for 24 hours, and rainfall was evaluated within 6 hour periods. In one domain of roughly 1000 $\times$ 1000 km centered over Iowa, 20 MCSs were simulated with both a 10 km version of the NCEP Eta model, and a 10 km version of the Weather Research and Forecasting (WRF) model, with both the Kain-Fritsch (KF) and Betts-Miller-Janjic (BMJ) convective schemes used in each model. In the other domain covering the International H_20 Project (IHOP) region of the Central United States, a 12 km version of the WRF model was run with 18 different combinations of convective, PBL and microphysical schemes to simulate 8 MCS events occurring during the 2002 IHOP period. Specifically, the BMJ and KF convective schemes were used, along with a fully explicit run. Both the Eta and MRF PBL packages were used. For explicit microphysics, the Lin et al. (MP2), NCEP 5-class (MP4) and Ferrier (MP5) schemes were used.

In experiments over the Iowa domain, it was found that Equitable Threat (ET) scores were generally similar on average between the Eta and WRF models. Runs with the BMJ scheme in the Eta model earned slightly higher ET scores than those with the KF scheme, but enough variability was present that the results were not statistically significantly different (in a Wilcoxon signed-rank test). In the WRF runs, both schemes earned comparable scores. Of interest, spread ratios (Stensrud and Wandishin 2000) indicated more similarity in the rainfall forecasts from two different models having the same convective scheme than in the same model running two different convective schemes. This result supports previous findings about the prominent role the convective parameterization plays in the simulation of rainfall during the warm season.

In tests over the IHOP domain, it was found that no particular set of physical parameterizations (out of 18 possibilities) consistently resulted in the best rainfall forecast skill. Table 1 shows ET scores for the first 6 hours of forecasts when the WRF model was initialized using the LAPS "hot start" diabatic initialization. During this time, the highest ET scores for lighter rainfall thresholds were associated with runs that did not use a convective scheme. For heavier amounts, higher scores occurred in some of the KF and BMJ runs, but varied as a function of the microphysical scheme. At later times in the 24 hr integrations, ET scores decreased and results changed so that overall, no particular convective, PBL, or microphysical scheme was favored. These results suggest that the combination of WRF physical configurations may yield a useful ensemble, assuming sufficient spread is present.

Standard deviations were computed for the ET scores when one physical process was varied while the other two were held constant (not shown). These results suggest that the convective scheme has a bigger impact on the forecast for light rainfall amounts at early times (prior to 12 h) but that the microphysical and PBL schemes have a comparable influence by the 18-24 h forecast period. For heavier rainfall amounts, the microphysical and convective schemes exert similar influences at all times, and the PBL scheme has less impact.

	Precipitation Threshold (mm)			
Model Physics	.254	2.54	12.7	25.4
BMJ-ETA-MP2	.246	.167	.100	.053
BMJ-ETA-MP4	.249	.182	.070	.026
BMJ-ETA-MP5	.249	.177	.079	.029
BMJ-MRF-MP2	.249	.179	.099	.054
BMJ-MRF-MP4	.249	.178	.100	.046
BMJ-MRF-MP5	.252	.180	.074	.038
KF-ETA-MP2	.235	.187	.077	.055
KF-ETA-MP4	.242	.201	.066	.033
KF-ETA-MP5	.272	.205	.090	.063
KF-MRF-MP2	.255	.196	.073	.059
KF-MRF-MP4	.265	.211	.067	.041
KF-MRF-MP5	.276	.206	.075	.038
NC-ETA-MP2	.349	.247	.086	.044
NC-ETA-MP4	.327	.215	.048	.022
NC-ETA-MP5	.298	.203	.055	.041
NC-MRF-MP2	.308	.201	.066	.039
NC-MRF-MP4	.304	.191	.057	.029
NC-MRF-MP5	.311	.208	.057	.032

Table 1: ET scores averaged for 8 IHOP cases for 18 WRF physical configurations (BMJ, KF, and no convective schemes, ETA and MRF PBL schemes, and MP2-Lin et al., MP4-NCEP 5 class, and MP5-Ferrier microphysical schemes) for 4 rainfall thresholds in the 00-06 forecast hour period.

Initial tests of the use of the WRF runs as an ensemble show rather high areas under the Relative Operating Characteristic (ROC) curve during the early times for lighter rainfall amounts, with a peak value of over .8 in the first 6 hours for .254 mm of rainfall. The skill of the ensemble forecast does appear to be better than that of any single deterministic run, but the ensemble forecasts, like the deterministic ones, show little skill for heavier amounts (such as 12.7 mm).

In summary, we are finding that no particular combination of common physical parameterizations in the Eta and WRF models consistently results in a better rainfall forecast for warm season MCS events. The impact of the convective parameterization is so substantial that forecasts from two different models using the same convective scheme will typically resemble each other more than forecasts from the same model using varied convective schemes. This result could influence the design of short-range ensembles.

Acknowledgments

This work was supported by NSF grant ATM-0226059 and in part by funding from NOAA's Forecast Systems Laboratory.

References

Stensrud, D. J., and M. S. Wandishin, 2000: Correspondence and spread ratios in forecast verification. *Wea. Forecasting*, **15**, 593-602.

NWP research in Austria

T. Haiden
Central Institute for Meteorology and Geodynamics
thomas.haiden@zamg.ac.at

1. Operational forecast system

Operational limited area weather forecasts in Austria are made using version AL25 of the ARPEGE/ALADIN modelling system. ALADIN forecasts are made on two Central European domains, with horizontal resolutions of 12.1 km and 9.6 km, respectively. The number of levels in the vertical is 37 in both cases. The model is spectral, run in hydrostatic mode, with a semi-implicit, semi-Lagrangian advection scheme. Initial and boundary conditions are taken from the global model ARPEGE. A modified Bougeault scheme is used for deep convection, a first-oder closure for turbulent vertical transports, and the ISBA (Interaction Soil-Biosphere-Atmosphere) scheme is used to represent surface processes. Coupling frequency is 3 hours. Integrations up to +48 hours are performed twice a day.

2. Research

a. Numerical prediction of inversion fog and low stratus

The underprediction of low stratus capped by an inversion is a major forecasting problem in eastern central Europe. The negative bias in low cloud cover is one of the primary sources of error in 2m temperature forecasts during wintertime (Greilberger and Haiden, 2003). Low stratus events are typically of large scale in the horizontal, and quasi-stationary over several days. Radiation and vertical mixing are the dominant cloud forcing mechanisms. According to 1-d and 3-d modelling studies the underprediction of inversion cloudiness is due to a too smooth temperature profile across the inversion. Current work focuses on the development stage of the inversion, and on the comparison of first order and prognostic TKE turbulence closures in the prediction of inversion development. Also, alternative formulations for the cloudiness parameterizations are being tested (Kann, 2003; Haiden, 2004). The work is part of COST Action 722 ‘Short-Range Forecasting Methods of Fog, Visibility and Low Clouds’.

b. Deep convection triggering

The problem of the diurnal cycle of convective precipitation, i.e. that the precipitating stage is reached too early in NWP models, is well known. Previous studies with ALADIN have shown that using a prognostic deep convection scheme tends to improve the mesoscale precipitation structures but does not solve the timing problem as long as the trigger function is kept unchanged. Simply using CAPE triggering does not solve the problem either. Experiments are made with improved trigger functions which address more explicitly the convective inhibition (CIN) as well as cloud growth from Cu to Cu-cong into Cb (Wimmer, 2003).

c. Prediction of cold air pools and katabatic flows

The fact that NWP models usually employ a terrain-following coordinate system at low levels poses a problem in the forecasting of cold air pools in complex terrain. Problems also occur as

a result of the use of envelope orography, such that generally cold air pools contained within alpine basins are not simulated well. In an ongoing research initiative, the mechanisms of katabatic flow formation and basin cooling are investigated in detail (Haiden, 2003a; Haiden, 2003c; Haiden and Whiteman, 2004; Whiteman et al., 2004).

d. Prediction of heavy rainfall

As a response to the August 2002 floods in Central Europe, which severely affected large parts of Austria (Haiden, 2003b), research has started on combining radar data and model results in the nowcasting of rainfall amounts for hydrological applications. The orographic component of heavy precipitation is studied by Wang (2003) using different initial conditions based on data gathered during the Mesoscale Alpine Programme (MAP).

e. High-resolution non-hydrostatic simulations

In order to improve the simulation of terrain-related phenomena, experiments are made with a high resolution (2-3 km) non-hydrostatic version of the ALADIN model (Stadlbacher, 2003). The performance of high-resolution wind and precipitation forecasts is compared to the operational one (10 km), as well as to statistically downscaled wind forecasts.

References

Greilberger, S., and T. Haiden, 2003: T2m nowcasting. *ALADIN Newsletter, 23,* 136-137.

Haiden, T., 2003a: On the pressure field in the slope wind layer. *J. Atmos. Sci.*, **60,** 1632-1635.

Haiden, T., 2003b: On the performance of ALADIN during the August 2002 floods. *ALADIN Newsletter, 23,* 191-193.

Haiden, T., 2003c: Evaluation of analytical predictions of katabatic flow on a low-angle slope. *Preprints, ICAM and MAP Meeting,* Brig, Switzerland, 150-152.

Haiden, T., and C. D. Whiteman, 2004: Katabatic flow mechanisms on a low-angle slope. *J. Appl. Meteor*. (submitted)

Haiden, T., 2004: Improvement of low stratus forecasts. Proceedings, *13th ALADIN Workshop,* Prague.

Kann, A., 2003: 1 month parallel run with Seidl-Kann cloudiness scheme. ALADIN Newsletter 24.

Seidl, H., 2003: Derived Quantities, Filtering and Model Consistency at High Resolution (Aladin vs. ECMWF validation). Proceedings of the 13th International ALADIN Workshop, Prague.

Stadlbacher, K., 2003: Qualitative evaluation of ALADIN non-hydrostatic dynamics on high resolution. Proceedings, 4th ALATNET Seminar, HMS.

Wang, Y., 2003: Impact of the topography and LBC on the ALADIN precipitation forecast. ALADIN Newsletter 24

Whiteman, C. D., T. Haiden, B. Pospichal, S. Eisenbach and R. Steinacker (2004): Minimum temperatures, diurnal temperature ranges and temperature inversions in limestone sinkholes of different size and shape. *J. Appl. Meteor*. (submitted)

Wimmer, F., 2003: Convective activity in ALADIN-VIENNA. ALADIN-LACE report, 6p.

THE AUSTRALIAN AIR QUALITY FORECASTING SYSTEM

G. D. Hess[1], M. E. Cope[2,3], S. Lee[2], K. Tory[1], M. Burgers[1,4], P. Dewundege[4] and M. Johnson[5]

[1]Bureau of Meteorology Research Centre, Melbourne, Victoria, Australia, [2]CSIRO Atmospheric Research, Aspendale, Victoria, Australia, [3]CSIRO Energy Technology, Lucas Heights, New South Wales, Australia, [4]Environment Protection Authority of Victoria, Melbourne, Victoria, Australia, [5]New South Wales Department of Environment and Conservation, Lidcombe NSW, Australia.
E-mail: d.hess@bom.gov.au

The Australian Air Quality Forecasting System (AAQFS) is a joint project between the Bureau of Meteorology (BoM), CSIRO Atmospheric Research (CAR), CSIRO Energy Technology (CET), the Environment Protection Authority of Victoria (EPA Victoria) and the New South Wales NSW Department of Environment and Conservation (NSW DEC) to develop a high-resolution air quality forecasting system. The initial development of AAQFS was funded by the Air Pollution in Major Cities Program (sponsored by Department of Environment and Heritage).

The project has a number of specific goals: to provide the ability to generate 24/36-hour air quality forecasts twice per day (available 9 am and 3 pm); provide forecasts for a range of air pollutants including oxides of nitrogen (NO_x), ozone (O_3), sulfur dioxide (SO_2), carbon monoxide (CO), benzene (C_6H_6), formaldehyde (CH_2O) and particulate matter (PM10 and PM2.5); provide forecasts at a resolution sufficient to consider suburban variations in air quality; and to provide the ability to generate simultaneous forecasts for a 'business-as-usual' emissions scenario and a 'green emissions' forecast. The latter scenario may correspond to minimal motor vehicle-usage, for example, and which could be used to indicate the reduction in population exposure that could result from a concerted public response to a forecast of poor air quality for the next day.

The AAQFS consists of five major components: a numerical weather prediction (NWP) system, an emissions inventory module (EIM), a chemical transport module (CTM) for air quality modelling, an evaluation module, and a data archiving and display module.

The BoM's operational Limited Area Prediction System (LAPS) has been adapted for the AAQFS NWP component. Comprehensive numerics and physics packages are included and recent work has paid special attention to the resolution and treatment of surface processes. The model has 29 vertical levels and a horizontal resolution of 0.05° (covering the State of Victoria and most of New South Wales). This model is nested in LAPS at 0.375^o resolution, which in turn is nested in the BoM global model, GASP.

EPA Victoria and CSIRO, with support from NSW DEC, have developed the emissions inventory. The inventory component includes estimates of size-fractionated and speciated particle emissions, 0.01° gridded area sources over the densely populated regions and meteorologically-dependent emissions that are generated based on LAPS predictions.

The CTM has been custom-built for the project using state-of-the-art methodologies. A notable inclusion to the CTM is the Generic Reaction Set photochemical mechanism, a highly condensed (7 species and 7 reactions) photochemical transformation mechanism featuring minimal computational overhead. Parallel tests of a more comprehensive photochemistry, Carbon Bond IV, are currently being conducted for a second oxidant season. Particle transformation is modelled by a sectionally-based particle scheme. The transport fields are updated every 60 minutes. The CTM has 17 vertical levels, and simulations use a 0.05° outer grid, with nested 0.01° inner grids for major urban areas.

While the focus of the AAQFS to date has been the forecasting of urban air quality, other applications have been considered. The AAQFS has been adapted to forecast dust storms and the transport of bushfire smoke. Recent work (cf. Fig. 1 and 2) has focused on verification of peak 1-

hour ozone forecasts and provision of an initial benchmark for investigating the limits of predictability for air quality in the Sydney and Melbourne regions by looking at the dependence of the forecasts on spatial scale, the starting time, and the sophistication of the photochemical mechanism.

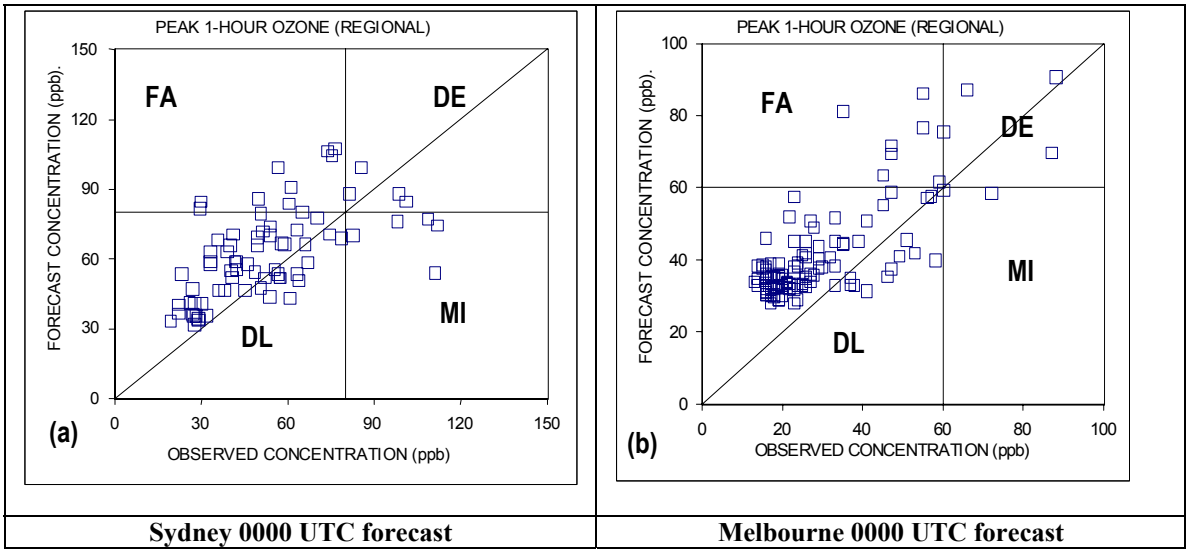

Figure 1. Scatter plots of regional-scale forecasts (uncoupled in space) and observed daily peak 1-hour ozone concentration for (a) the Metropolitan Air Quality Study Region (Sydney and environs) and (b) the Port Phillip Control Region (Melbourne and environs). The upper left quadrant indicates the region of false alarms, FA, the lower left quadrant, DL, the region of detection of low and medium concentration events, the lower right quadrant, MI, the region of missed forecasts, and the upper right quadrant, DE, the region of detection of extreme concentration events. The diagonal lines indicate a perfect forecast.

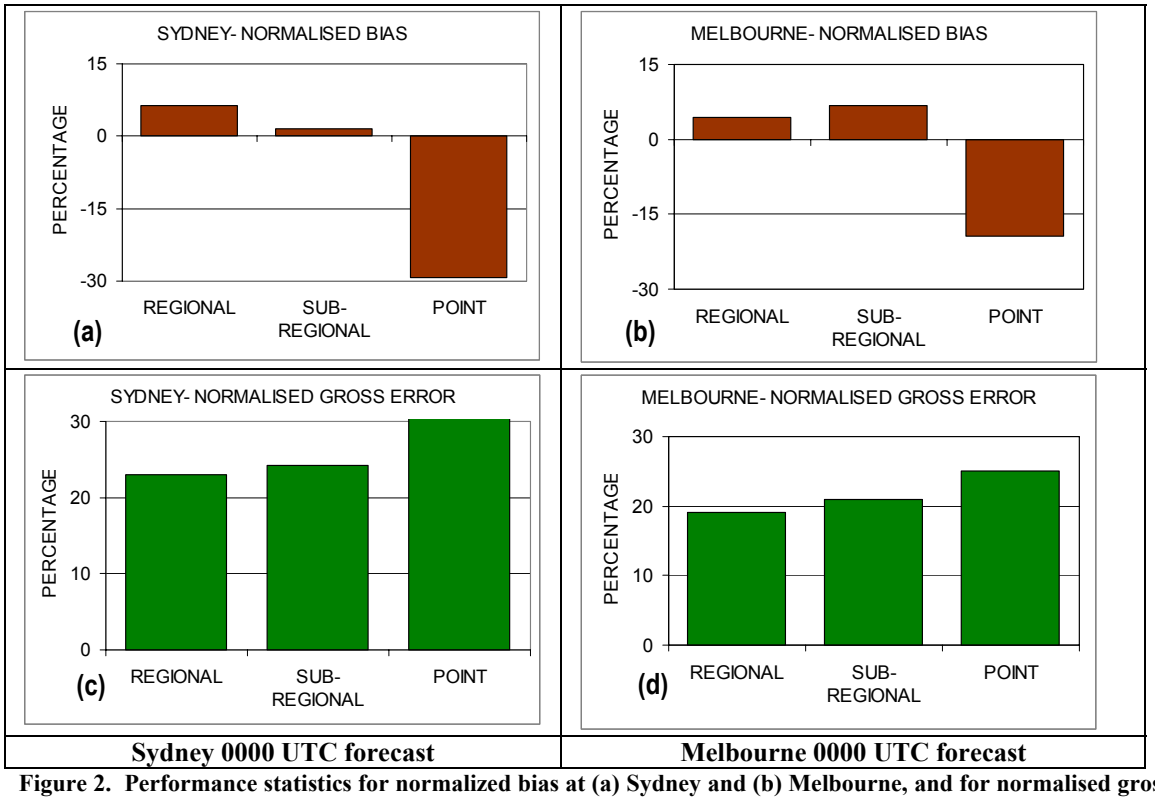

Figure 2. Performance statistics for normalized bias at (a) Sydney and (b) Melbourne, and for normalised gross error for (c) Sydney and (d) Melbourne for the forecasts of daily peak 1-hour ozone, as a function of the spatial scale of the forecasts.

Use of high-resolution dynamical adaptation for the extreme wind estimate

Stjepan Ivatek-Sahdan, Meteorological and Hydrological Service, Grič 3, HR-10000 Zagreb, Croatia, ivateks@cirus.dhz.hr
Martina Tudor, Meteorological and Hydrological Service, Grič 3, HR-10000 Zagreb, Croatia, tudor@cirus.dhz.hr

Prior to the intorduction of the high-resolution dynamical adaptation, local strength of bura has not been forecasted by operational models in the Croatian Meteorological Service. The forecast of bura was subjective, depended on forecaster's experience and local knowledge. In addition, the insufficient spatial density of measurements often prevented detection of the most affected areas

The high-resolution dynamical adaptation was developed by Žagar and Rakovec (1999). It is performed in the following way. The 8-km resolution wind field is interpolated to 2-km grid and then dynamically adapted using ALADIN model. The model is run for 30 min with 60-sec time-step at 2-km resolution. During this run part of the physics describing the moist and radiation processes is switched-off and the number of levels in the upper troposphere and stratosphere is reduced. The high resolution dynamical adaptation significantly improves the large scale wind field when the main forcing is exerted by the pressure gradient over mountains, as it is the case with bura. However, it can not predict local thermal circulation nor circulation caused by convection processes.

For the purpose of the construction of the new highway in the area with strong bura, the extreme wind speeds have to be estimated. The spatial density of wind measurements was insufficient for the task; the measurements were available only at the two locations, from Maslenica and Pag bridges. The extreme wind speeds in that area belong to bura episodes. Using operational 2-km resolution dynamical adaptation, expected wind speeds were estimated for extreme bura cases.

When the construction of the road began, additional automatic meteorological stations were set up. The results from 2-km resolution dynamical adaptation forecast were compared to the measurements at new stations (Figure 1). For one case of bura, operational wind speed forecasts were compared to the two alternatives (Figure 2);

- the dynamical adaptation was run with full physics
- the full 48 hour forecast was run with 2-km resolution

The choice of the operational dynamical adaptation set-up for the estimation of the extreme wind speed was good.

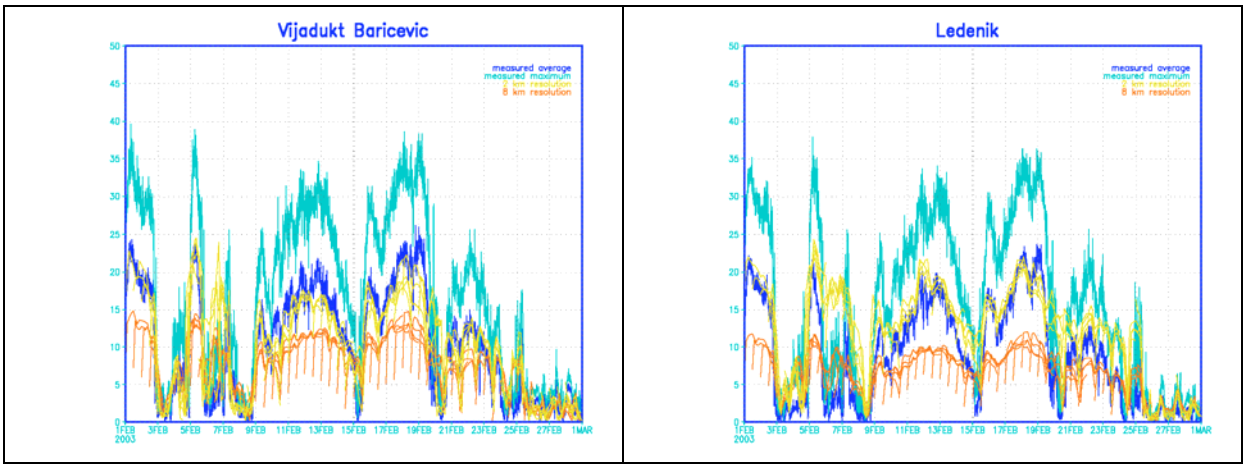

Figure 1. Measured wind speed for the Baričević Viaduct (left) and the Ledenik Tunnel (right) automatic stations and modeled data from the closest model point for February 2003. Measured 10 min average wind speed (dark blue), 10 min maximum (light blue), all model forecasts for February 2003 (00 and 12 UTC runs) with 8-km resolution (orange) and 2-km resolution operational dynamical adaptations (yellow). The 2-km resolution predicts the occurrence and strength of the 10-min average wind speed well.

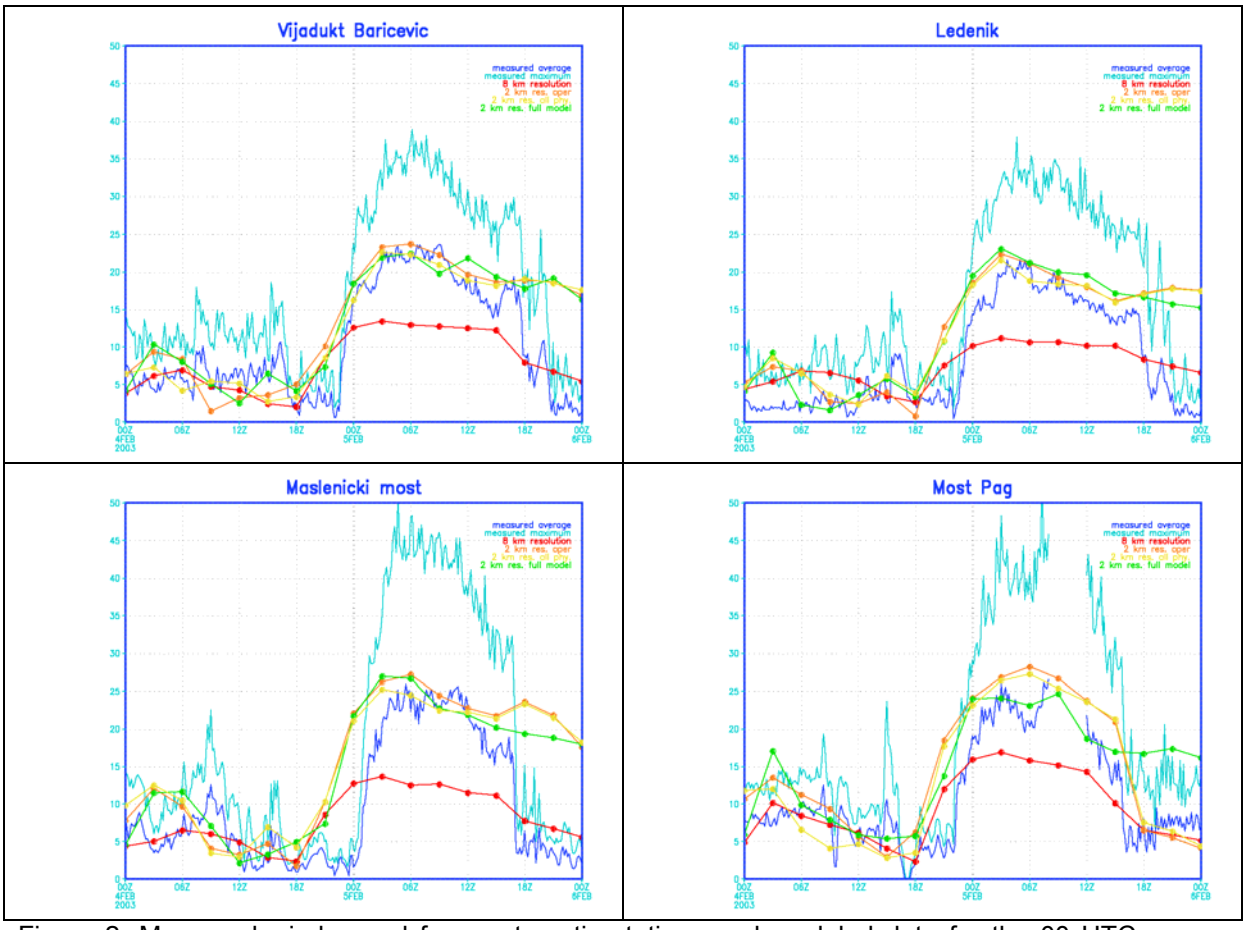

Figure 2. Measured wind speed from automatic stations and modeled data for the 00 UTC run on February 4th 2003 from the closest model point. Measured 10 min average wind speed in m/s (dark blue), 10 min maximum (light blue), 8-km resolution model forecast (red), 2-km resolution dynamical adaptations; operational (orange), using whole physics package (yellow) and 2-km resolution 48-hour model integration (green).

The high resolution dynamical-adaptation approach used in the operational suite works well when the wind is strong enough to overcome the circulation induced by local thermal or convection induced circulation. Therefore, it represents a powerful tool for estimation of the expected wind speed during the extreme weather events induced by pressure gradient forcing.

References

Žagar, M. and J. Rakovec, 1999: Small-scale surface wind prediction using Dynamical adaptation. *Tellus*, **51A**, 489-504.

Application of 3D regional transport model for study of methane formation mechanisms over large industrial area (Saint Petersburg)

Jagovkina S.V.[1] , Karol I.L.[1] , Zubov V.A., [1] ; Lagun V.E.[2], Reshetnikov A.I..[3], Paramonova N.N..[3], Privalov V.I., Poberovsky A.V.[4], Makarova M.V.[4]

[1] Main Geophysical Observatory, Karbyshev str. 7, St.-Petersburg, 194021, Russia, svetlana@main.mgo.rssi.ru.
[2] Arctic and Antarctic Research Institute, Bering str. 38, St. Petersburg, 199397, Russia
[3] Res. Center of Remote Sensing of Atmosphere, Karbyshev str. 7, St.-Petersburg, 194021, Russia
[4] St.-Petersburg State University, Uljanovskaia str., Petrodvorez, St.-Petersburg, 198904, Russia

Combining atmospheric transport model [1] with multiyear methane measurements (high precision methane concentrations [2] and methane column content [3]) allows to obtain high quality information about methane distribution in troposphere and its variability. A 3-D regional transport model of high spatial resolution ($\Delta y=0.25^0$ = 27 km along longitude, $\Delta x = 0.5^0$ (~18-32 km) along latitude) is developed, adjusted and applied for study of methane budget mechanisms formation and emission assessment over industrial Saint-Petersburg area (55-65^0 N; 20-40^0 E). The vertical structure of the model is 10 unevenly spaced layers inside the boundary layer (up to 1 km) and 10 one-km layers in the above troposphere. Time step is 5 min for the gas transport calculations. The wind fields for the troposphere above PBL are updated from the 6-hourly ECMWF databases. The methane surface boundary fluxes are prescribed on the base of published data about methane emissions from North mires and methane fluxes from urban area of St.-Petersburg [4,5].

The multiyear series of observations are used, obtained by spectroscopic (1996-2001) and gas chromatographic methods (1987-2003). The applied model allows to assimilate both indicated above kinds of methane measurements.

The model was run for different seasons for periods of ground based (Voeikovo) and column (Petrodvorez) measurements, for instance, Figure 1 demonstrates geographical distribution of surface layer methane concentration and Figure 2 presents total methane column field for the same day over St.-Petersburg region.

Developed approach allows to estimate the input of natural and anthropogenic methane fluxes and long range atmospheric transport into regional methane budget formation and to explain the anomalies of methane content connected with current weather conditions.

This work is supported by Grant of Russian Foundation for Basic Research 02-05-64711.

References

1. Jagovkina S., Karol I., Zubov V., Lagun V., Reshetnikov A., Rozanov E. Reconstruction of the Methane Fluxes from the West Siberia Gas Fields by the 3D Regional Chemical Transport Model. Atmospheric Environment, 2000, 34, 5319-5328.
2. Zinchenko A.V., Paramonova N.N., Privalov V.I., Reshetnikov A.I. Estimation of methane emission from St.-Petersburg area using data of methane concentrations in the air near surface. Russian Meteorology and Hydrology, 2001, 5, 35-49.

3. Makarova M.V., Poberovsky A.V., Timofeev Yu.M. Spectoscopic measurements of total methane content in St.-Petersburg area. Atm. & Ocean Phys., 2001, 37, N1, 67-73.
4. Nilsson M. et all. Methane emission from Swedish mires: National and regional budgets and dependence on mire vegetation. J. Geophysical Research., 2001, 106, 20847-20860.
5. Christensen T.R., Ekberg A., Strom L., Mastepanov M. et al. Factors controlling large scale variations in methane emissions from wetlands. Geoph. Research Letters, 2003, 30, 67-1- 67-4.

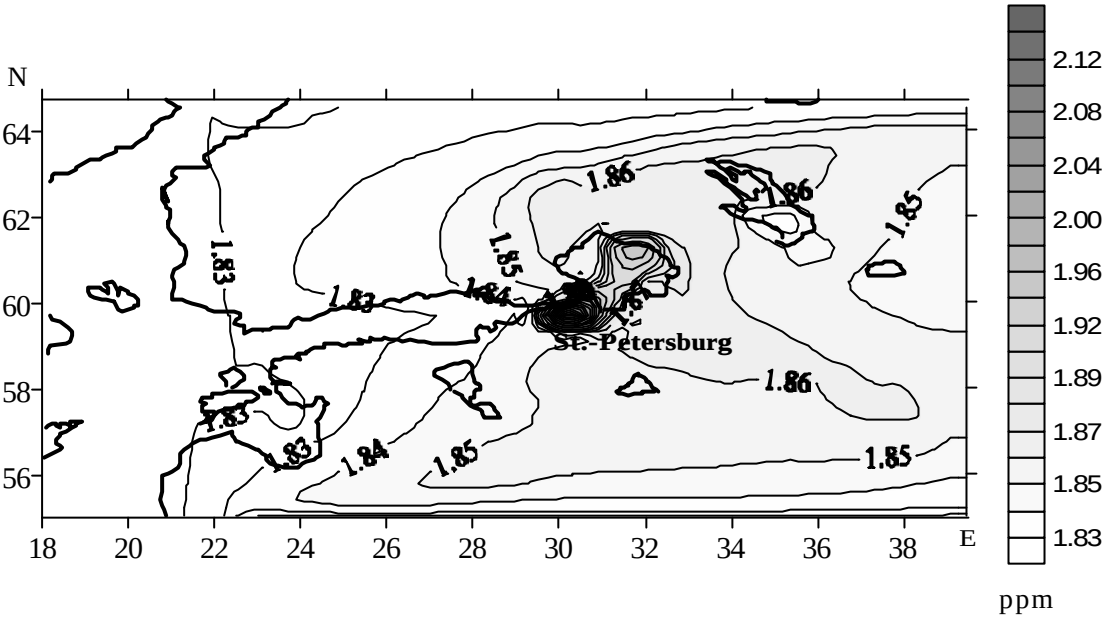

Fig. 1 Geographical distribution of methane concentration (ppm) at the altitude h ~ 15 m for 4 February, 1996

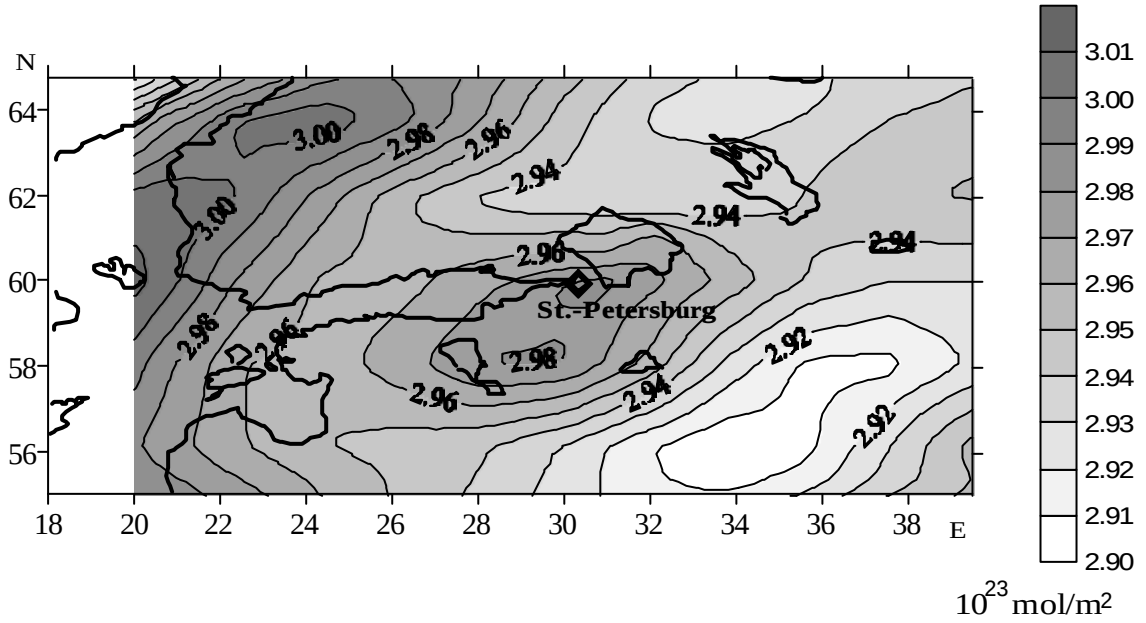

Fig. 2 Geographical distribution of methane column content (mol/m^2) up to 11 km for 4 February, 1996

ENSEMBLE FORECASTS OF TORNADIC THUNDERSTORMS

Fanyou Kong[1] and Kelvin K. Droegemeier[1,2],
[1]*Center for Analysis and Prediction of Storms, and* [2]*School of Meteorology, University of Oklahoma, Norman, OK 73019, USA*
fkong@ou.edu

1. Research Activity Overview

Ensemble forecasting has proven valuable in medium-range global model forecasts (6-10 days) and now is a foundation in major operational forecast centers around the world (Kalnay 2003). Short-range ensemble forecasting (SREF, ~40 km resolution, 1-3 days) with limited-area models has been underway for some time (Du and Tracton 2001), and interest now is growing in storm-scale ensemble forecasts (Elmore et al. 2003; Levit et al. 2004; Kong et al. 2004). Still, the effectiveness of the stochastic-dynamic approach on the storm-scale has yet to be fully explored, particularly the degree to which theories of error growth and initial condition specification at larger scales apply to smaller ones.

Current activities at the Center for Analysis and Prediction of Storms (CAPS) involve the use of the Advanced Regional Prediction System (ARPS) to produce multiple-resolution ensemble forecasts of severe thunderstorms. One such case simulated is a tornadic thunderstorm complex that occurred in the vicinity of Fort Worth, TX on 28-29 March 2000. Because storm-scale forecasting generally requires very fine horizontal grid spacing (1-3 km), nested grids must be used. In this study, we use 24-km, 6-km, and 3-km spacing for the coarse, medium, and fine resolution domains, respectively. The fine 3-km domain is centered over Fort Worth with sufficient coverage for the features of interest. The 24-km domain consists of 238×150 horizontal grid points; while the other two consist of 180×180 each. All use 53 terrain-following vertical layers, with nonlinear stretching from 20 m at the ground to approximately 800 m at the top. For each nested domain, a five-member scaled-lagged average forecasting (SLAF) ensemble (one control forecast plus 4 perturbed members) (Ebisuzaki and Kalnay 1991) is generated. To construct the latter, the perturbation between a previous ARPS forecast and the current analysis is scaled based upon time (error growth) and then added to and subtracted from the analysis to form two (paired) members. A 5-member SLAF requires two successive previous ARPS forecasts.

Nested grids complicate the construction of ensemble forecasts because no unique strategy exists to link the grids. Several approaches have been tested so far. One of them, for instance, only has the control runs of the 6-km ensemble and 3-km ensemble nested successively from the coarser grids. The perturbed members are constructed directly for the two previous 24-km ARPS forecasts (interpolated onto 6-km and 3-km grids, respectively) and the current analyses on the finer grids.

For both the 24-km and 6-km ensembles, both cumulus parameterization and explicit ice-phase microphysics are used. For the 3-km ensemble, only the explicit microphysics scheme is applied. For the finer grids, WSR-88D Level III reflectivity data are included in the ARPS data assimilation system (ADAS) in addition to other observation data.

2. Storm-Scale Ensemble Results

For each grid, individual member exhibits diversity and captures the major precipitation systems. The hourly rainfall probability maxima from 3-km grid are reasonably well aligned with the rainfall cores in the Stage IV rainfall map (figures not shown). In general, the 3-km ensemble contains significantly greater detail compared to its coarser grid counterparts, and generally agrees more closely with reality. Though very simple, the SLAF ensembles do show very promising storm scale forecasting skill.

Figure 1 shows example ensemble forecast products from the 3-km grid, along with the WSR-88D radar reflectivity. At 3-km grid spacing, convection is explicitly resolved by the microphysics scheme, though this grid spacing is toward the upper limit of that deemed practicable for application to deep convection. Owing to the spatially intermittent nature of deep convection, the ensemble mean reflectivity forecast covers a much broader area than any of the individual forecasts, and each storm tends to be much weaker. For this reason, the ensemble probabilities might be more useful. As shown in Figure 1, the conditional probabilities of surface reflectivity exceeding 45 dBZ compare very favorably with the WSR-88D (KFWS) reflectivity map, though the low probability echoes over the southeastern portion of the domain are not shown in KFWS radar.

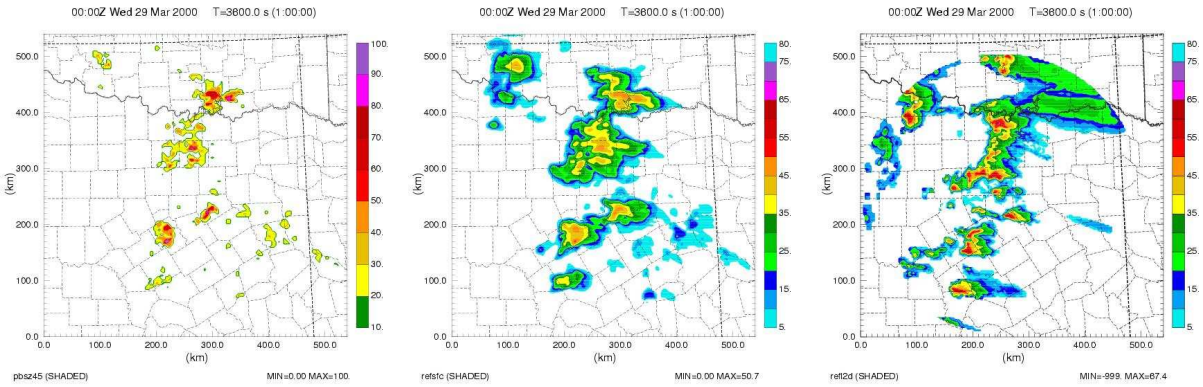

Figure 1. 1-h forecast probability of model-equivalent radar reflectivity ≥45 dBZ (left) and ensemble mean (center) from 3-km ensemble, and the Fort Worth WSR-88D lowest tilt reflectivity (right), valid 0000 UTC 29 March 2000.

References

Du, J., and M. S. Tracton, 2001: Implementation of a real-time short-range ensemble forecasting system at NCEP: An update. *Preprints, 9th Conf. on Mesoscale Processes*, Amer. Meteor. Soc., 355-356.

Ebisuzaki, W., and E. Kalnay, 1991: Ensemble experiments with a new lagged average forecasting scheme. WMO Report #15.

Elmore, K. L., S. J. Weiss, and P. C. Banacos, 2003: Operational ensemble cloud model forecasts: Some preliminary results. *Wea. And Forecasting*, **18**, 953-964.

Kalnay, E., 2003: *Atmospheric Modeling, Data Assimilation and Predictability*. Cambridge Press, 341pp.

Kong, F.-Y., K. K. Droegemeier, V. Venugopal, and E. Foufoula-Georgiou, 2004: Application of scale-recursive estimation to ensemble forecasts: A comparison of coarse and fine resolution simulations of a deep convective storms. *Preprints, 20th Conf. on Wea. Analysis and Forecasting/16th Conf. on Num. Wea. Prediction*, Amer. Meteor. Soc..

Levit, N. L., K. K. Droegemeier, and F. Kong, 2004: High-resolution storm-scale ensemble forecasts of the 28 March 2000 Fort Worth Tornadic storms. *Preprints, 20th Conf. on Wea. Analysis and Forecasting/16th Conf. on Num. Wea. Prediction*, Amer. Meteor. Soc..

WATER VAPOR SOURCES AND SINKS,
AND HYDROMETEOR LOADING IN THE ETA MODEL

Fedor Mesinger and Lazar Lazic*

The eta system equations of Mesinger (1984; also in Mesinger at al., 1988) were arrived at with the assumptions that (a) effects of sources and sinks of water vapor, and of the presence of liquid water/ice are neglected, (b) that discretization to follow will be of the step-mountain type, so that the eta vertical velocity at the ground surface is zero, and (c) that the hydrostatic approximation is made. The removal of (b) was discussed in Mesinger (2000). The objective here is to generalize equations so that the assumption (a) be removed.

We shall introduce the generalizations involved one at a time, starting with the effects of water vapor sources and sinks in the continuity equation, and then moving on to the water/ice loading effects in the hydrostatic and the pressure tendency equations.

For reference, we shall first write down the eta system continuity equation with no mass sources or sinks, (2.5) in Mesinger et al. (1988),

$$\frac{\partial}{\partial\eta}\left(\frac{\partial p}{\partial t}\right)+\nabla\cdot\left(\mathbf{v}\frac{\partial p}{\partial\eta}\right)+\frac{\partial}{\partial\eta}\left(\dot{\eta}\frac{\partial p}{\partial\eta}\right)=0. \tag{1}$$

We want to allow for the sources and sinks of water vapor, such as tend to be assumed by various precipitation schemes. Following a standard mass budget consideration , and using q for specific humidity, we arrive at

$$\frac{\partial}{\partial\eta}\left(\frac{\partial p}{\partial t}\right)+\nabla\cdot\left(\mathbf{v}\frac{\partial p}{\partial\eta}\right)+\frac{\partial}{\partial\eta}\left(\dot{\eta}\frac{\partial p}{\partial\eta}\right)-\frac{dq}{dt}\frac{\partial p}{\partial\eta}=0. \tag{2}$$

Note a slight difference compared to Savijarvi's (1995) sigma system equation: in (2) q is specific humidity, as opposed to the mixing ratio of Savijarvi.

To obtain the surface pressure tendency equation we need to integrate (2) from the top to the bottom of the model atmosphere. To handle the singularity at the surface, we integrate only to $\eta_S-\varepsilon$, ε being small, obtaining

$$\frac{\partial p_S}{\partial t}=-\int_0^{\eta_S-\varepsilon}\nabla\cdot\left(\mathbf{v}\frac{\partial p}{\partial\eta}\right)d\eta+\int_0^{\eta_S-\varepsilon}\frac{dq}{dt}\frac{\partial p}{\partial\eta}d\eta+gE, \tag{3}$$

as a replacement of (2.8) in Mesinger et al. (1988). Here E is the mass of water vapor evaporated into the atmosphere per unit area and unit time.

Integrating (2) from 0 only to η, and rearranging terms, we obtain

$$\dot{\eta}\frac{\partial p}{\partial\eta}=-\frac{\partial p}{\partial t}-\int_0^{\eta}\nabla\cdot\left(\mathbf{v}\frac{\partial p}{\partial\eta}\right)d\eta+\int_0^{\eta}\frac{dq}{dt}\frac{\partial p}{\partial\eta}d\eta. \tag{4}$$

Note that this replaces (2.9) of Mesinger et al. (1988).

Various hydrometeors if carried in a model, e.g., cloud water/ice, add weight to columns of air, affecting pressure. The total mass in a volume element as above is then

$$m_t=m_d+m_v+m_w, \tag{5}$$

where m_w is the mass of hydrometeors in the volume. A prognostic variable of the Eta is ÒspecificÓ cloud water/ice

$$w\equiv m_w/\left(m_d+m_v\right). \tag{6}$$

It is convenient to define an effective density, the density of the mixture of moist air and hydrometeors,

$$\rho_{eff}\equiv m_t/V. \tag{7}$$

Combined with (5) and (6), this gives

* Corresponding author: Lazar Lazic, Dept. Meteorology, Univ. Belgrade, Serbia. E-mail: lazar@ff.bg.ac.yu

$$\rho_{eff} = \rho(1+w). \qquad (8)$$

Use of (8) in the hydrostatic equation, and in the mass convergence terms of the pressure tendency equation, instead of the air density, will account for the effects of the hydrometeor loading on pressure.

Given that in the Eta code the evaporated water vapor is not added explicitly to the atmosphere but instead the latent heat flux is used as a boundary condition for the vertical diffusion of moisture, the total column water vapor needs to be calculated before and after the diffusion loop, and the evaporation obtained as the difference between the two.

Initial conditions for a sensitivity experiment we ran are those of 0000 UTC 18 January 1987, selected in an earlier study for their featuring the tropical cyclones *Connie* and *Irma* from the Australian Monsoon Experiment (AMEX). Figures below show total precipitation and central sea level pressure of *Connie* in our control and experiment during 48 h forecasts.

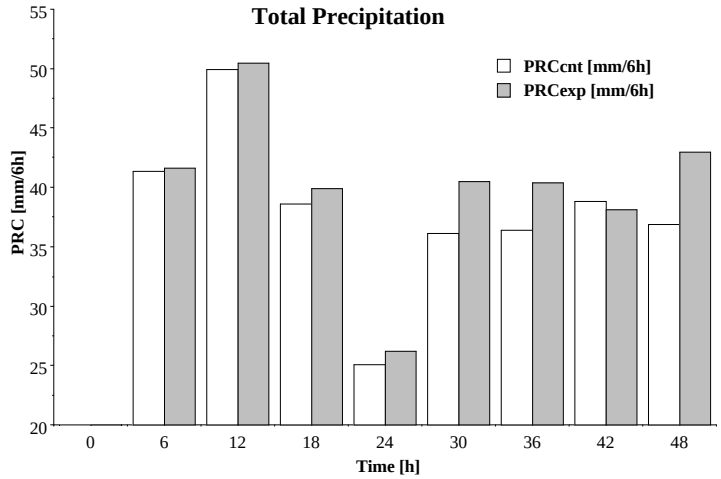

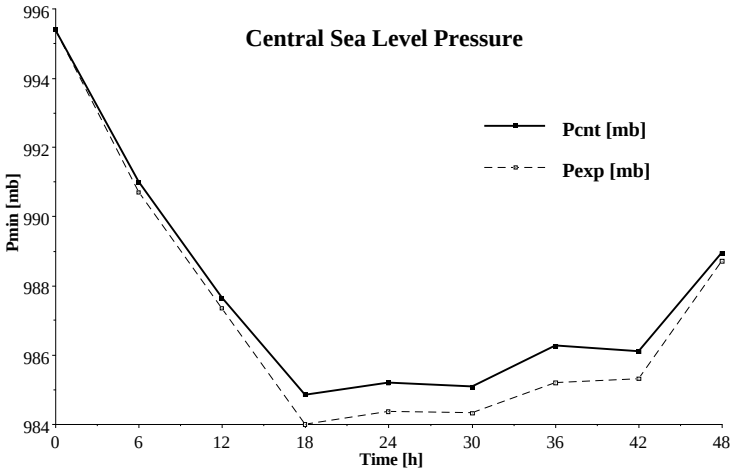

References

Mesinger, F., 1984: A blocking technique for representation of mountains in atmospheric models. *Riv. Meteor. Aeronautica*, **44**, 195-202

Mesinger, F., 2000: The sigma vs eta issue. Research Activities in Atmospheric and Oceanic Modelling, WMO, Geneva, CAS/JSC WGNE Rep. 30, 3.11-3.12.

Mesinger, F., Z. I. Janjic, S. Nickovic, D. Gavrilov and D. G. Deaven, 1988: The step-mountain coordinate: Model description, and performance for cases of Alpine lee cyclogenesis and for a case of an Appalachian redevelopment. *Mon. Wea. Rev.*, **116**, 1493-1518.

Savijarvi, H., 1995: Water mass forcing. *Contrib. Atmos. Phys.*, **68**, 75-84.

Operational implementation of regional ensemble forecasts

A. Montani, D. Cesari, C. Marsigli, F. Nerozzi, T. Paccagnella, S. Tibaldi

Regional Meteorological Service ARPA–SIM, Bologna, Italy
corresponding author: amontani@smr.arpa.emr.it

The forecast of localised and severe weather events (e.g. heavy rainfall, strong winds, cold temperature anomalies) is still nowadays a challenging problem, despite the more and more careful detection of precursors, developments and mature phase of this kind of events. Many weather centres have given more and more emphasis to the probabilistic approach, which enable to estimate the predictability of the atmospheric flow and assess the reliability of the deterministic forecast beyond the very short range. As to the use of limited–area models (LAMs), ARPA–SMR developed the Limited–area Ensemble Prediction System (LEPS). By means of a clustering–selection technique, ECMWF EPS members are first grouped into five clusters, then a Representative Member (RM) is selected within each cluster (Marsigli et al., 2001). The RMs provide both initial and boundary conditions for the integrations with a limited–area model, which is run five times (once per RM), so generating a small–size high–resolution ensemble for forecast ranges up to 120 hours. Hence, the typical probabilistic products (e.g. probability maps for rainfall rates or wind intensity exceeding particular thresholds) are produced on the basis of the information provided by the LAM integrations, each run being weighted according to the population of the cluster where the RM is selected. LEPS has been shown to perform better than EPS over a number of test cases and for forecast ranges between 48 and 120 hours (Montani et al., 2003a) in terms of estimate of precipitation intensity as well as in the detection of the regions most likely affected by heavy rain. These encouraging results opened the way to the experimental production of limited–area ensemble forecasts on a daily basis, the COSMO–LEPS project, which has recently started within the COSMO framework (COnsortium for Small–scale MOdelling; the members of the Consortium are Germany, Greece, Italy, Poland and Switzerland). This project aims to generate "short to medium–range" (48–120 hours) probabilistic predictions of severe weather events (based on the non–hydrostatic regional model Lokal Modell – LM) over a domain covering all countries involved in COSMO. An "experimental–operational" COSMO–LEPS suite (following the methodology described in Montani et al., 2003b) was set–up so as to produce probabilistic forecasts, based on LM nested on a selection of ECMWF EPS members.

As an example of COSMO–LEPS performance, we present the behaviour of the system for a heavy precipitation event occurred in November 2002 in Northern Italy. During the 24–hour period ending at 12UTC of 25 November 2002, rainfall values exceeding 100 mm/day were recorded all over the southern Alpine area, the highest amounts being observed in North-eastern Italy (above 150 mm/day). This caused widespread flooding as well as the overflow of several lakes in northern Italy. The main COSMO–LEPS product consists in combining the 5 LM deterministic runs using weights proportional to the population of the cluster where the RM providing initial and boundary conditions was selected. This enables the generation of probability maps on the basis of LM forecasts. For this case study, Fig. 1 shows the probability forecast (120–hour range) of 1–day rainfall exceeding 4 different thresholds: 20, 50, 100 and 150 mm. As to the two lowest thresholds (top–row panels), it can be noticed that all regions actually affected by the flood are highlighted as locations of heavy rainfall, with probability above 90% over North–western

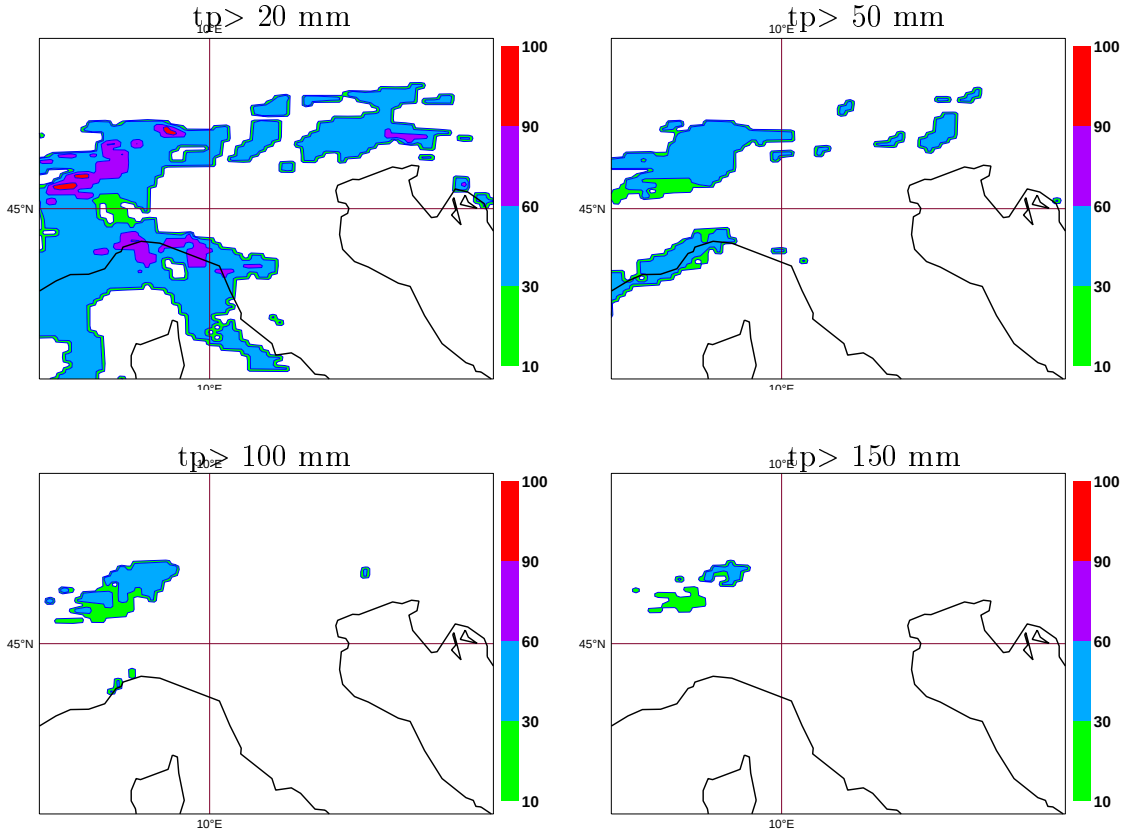

Figure 1: Probability maps of 24–hour rainfall exceeding 20 (top–left panel), 50 (top–right), 100 (bottom–left) and 150 mm (bottom–right) for COSMO–LEPS runs starting at 12UTC of 20 November 2002 (120–hour range). Contour intervals: 10%, 30%, 60%, 90%.

Italy for the 20 mm threshold. At the two highest thresholds (bottom–row panels), only the signal over north–western Italy "survives", with a probability of rainfall above 150 mm between 30% and 60%. Therefore, already at the 5–day range, the possibility of a intense and localised weather event over Northern Italy is highlighted, thus giving the possibility to issue preliminary warning to be either confirmed or dismissed on the basis of more recent forecasts. In these months, the experimental–operational part of COSMO–LEPS project is being accomplished. Deterministic and probability products based on LM are generated on a daily basis and disseminated to the meteorological services taking part to the COSMO consortium. The forecast accuracy of the products is being examined on the basis of several objective scores, which will evaluate both ability and shortcoming of the COSMO–LEPS system in a comprehensive way.

References

Marsigli C., Montani A., Nerozzi F., Paccagnella T., Tibaldi S., Molteni, F., Buizza R., 2001. A strategy for high–resolution ensemble prediction. Part II: limited–area experiments in four Alpine flood events. *Quart. J. Roy. Meteor. Soc.*, **127**, 2095–2115.

Montani A., Marsigli C., Nerozzi F., Paccagnella T., Tibaldi S., Buizza, R., 2003a. The Soverato flood in Southern Italy: performance of global and limited–area ensemble forecasts. *Nonlin. Proc. Geophys.*, **10**, 261–274.

Montani, A., Capaldo, M., Cesari, D., Marsigli, C., Modigliani, U., Nerozzi, F., Paccagnella, T., Tibaldi, S., 2003b. Operational limited–area ensemble forecasts based on the 'Lokal Modell'. ECMWF Newsletter No. 98. Available from: ECMWF, Reading, UK.

Direct evaluation of the buoyancy and consideration of moisture diffusion in the continuity equation in the JMA Nonhydrostatic Model

Kazuo Saito
Numerical prediction Division, 1-3-4 Otemachi, Chiyoda-ku, Tokyo 100-8122, Japan
ksaito@npd.kishou.go.jp

1. Introduction

The Japan Meteorological Agency (JMA) has been developing an operational nonhydrostatic model for regional NWP. This model (JMA-NHM) is based on the Meteorological Research Institute/Numerical Prediction Division unified nonhydrostatic model (http://www.mri-jma.go.jp/Dep/fo/mrinpd/INDEXE.htm). Among the three dynamical cores of JMA-NHM, the split-explicit time integration scheme (HE-VI scheme) is used for operation, considering the computational efficiency on the distributed memory parallel computer. Saito (2002) introduced a time splitting scheme of gravity waves where the computations of the buoyancy terms and vertical advection of the reference potential temperature are performed in the short time step in the HE-VI scheme. Saito (2003) introduced a time splitting scheme of advection terms where the higher-order advection terms are evaluated at the center of the leap-frog time step and the lower-order components are adjusted at each short time step. These schemes have significantly improved the computational stability of JMA-NHM.

In this report, we describe recent developments for JMA-NHM, which contribute to the mass conservation.

2. Direct evaluation of buoyancy

JMA-NHM defines the density as the sum of the masses of moist air and the water substances per unit volume as

$$\rho \equiv \rho_d + \rho_v + \rho_c + \rho_r + \rho_i + \rho_s + \rho_g = \rho_a + \rho_c + \rho_r + \rho_i + \rho_s + \rho_g , \qquad (1)$$

where subscripts *c, r, i, s, g* stand for the cloud water, rain, cloud ice, snow, and graupel, respectively. ρ_d is the density of dry air and ρ_v, that of water vapor. The buoyancy is defined as

$$BUOY \equiv \sigma \frac{\rho G^{\frac{1}{2}} \theta_m'}{\theta_m} g + (1-\sigma)(\overline{\rho} - \rho) g G^{\frac{1}{2}}. \qquad (2)$$

Here, σ is a switching parameter, which takes zero for direct computation of the buoyancy from the density perturbation and unity for conventional computation by the temperature perturbation. Using σ, vertical momentum equations can be expressed as

$$\frac{\partial W}{\partial t} + \frac{1}{mG^{\frac{1}{2}}} \frac{\partial P}{\partial z^*} + \sigma \frac{P}{mC_m^{\,2}} g = \frac{1}{m} BUOY - ADVW + RW. \qquad (3)$$

When σ=0, the pressure perturbation term (third term in the left-hand side) varnishes. The semi-implicit (HI-VI) scheme of JMA-NHM can use both σ=0 and σ=1, while σ=1 is assumed in the HE-VI scheme. In case of σ =1, the pressure perturbation term remains in the upper and lower boundary conditions for the vertically implicit pressure equation. In the Lorenz-type vertically staggered coordinate, it is difficult to determine this term at the upper and lower boundaries properly, and this problem yields a positive bias of mean pressure in the JMA-NHM.

In order to solve above problem, we modified the HE-VI scheme of JMA-NHM so that the buoyancy term can be evaluated by the density perturbation directly. In case of σ=0, the pressure perturbation term disappears in the vertical momentum equation (3), however, we have to teat the pressure perturbation implicitly for stable computation. The upper and lower boundary conditions of the vertically implicit pressure equation are as follows:

$$\delta_\tau W + \frac{1}{mG^{\frac{1}{2}}} \frac{\partial P^\beta}{\partial z^*} + \frac{g}{mC_m^{\,2}} P^\beta = \frac{1}{m} BUOY - (ADVW - RW) + (1-\sigma) \frac{g}{mC_m^{\,2}} P, \qquad (4)$$

where the terms with super-script β are treated implicitly. Above equation is formally similar to that for σ=1, while the additional last term of the right-hand side offsets the pressure perturbation term and the determination of pressure at upper and lower boundaries becomes less problematic. To split gravity waves, the density must be diagnosed at each short time step.

Figure 1 shows the domain-averaged mean sea level pressure of JMA-NHM whose initial time is 06 UTC 1 March 2003. Pressure of JMA-NHM with σ=1 increases after the start-up and is about 1.2 hPa higher than RSM, the outer model which supplies the lateral boundary conditions. On the other hand, pressure of JMA-NHM with σ=0 well follows that of RSM.

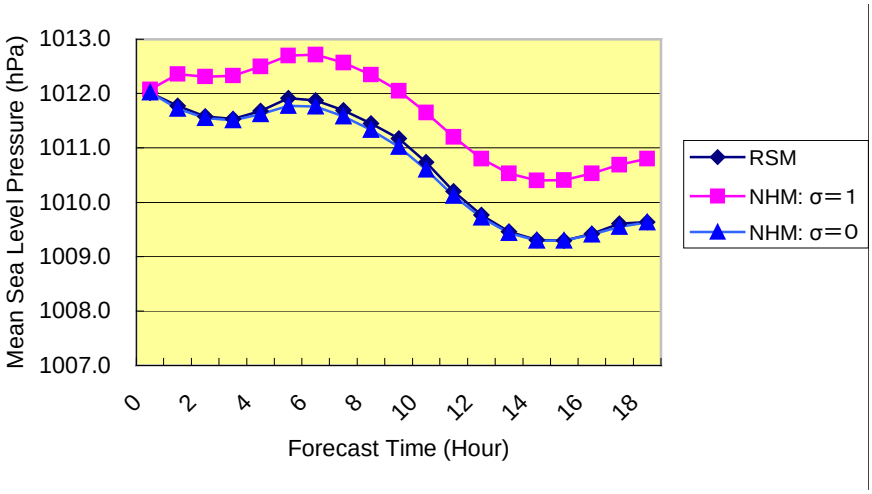

Fig. 1. Time sequence of the mean sea level pressure of JMA-NHM and RSM. Domain-averaged values for area of the JMA Mesoscale Model are shown. Initial condition for JMA-NHM is Meso 4D-Var analysis at 06 UTC 1 March 2003.

3. Consideration of moisture diffusion in the continuity equation

Since the density is defined by Eq. (1), JMA-NHM considers the fall-out of precipitable water substances in the continuity equation as

$$\frac{\partial \rho}{\partial t}+\frac{\partial \rho u}{\partial x}+\frac{\partial \rho v}{\partial y}+\frac{\partial \rho w}{\partial z}=\frac{\partial}{\partial z}(\rho_a V_r q_r+\rho_a V_s q_s+\rho_a V_g q_g). \qquad (5)$$

Here, V is the mass-weighted bulk terminal velocity for precipitable water substances and q the mixing ratio. Volume integrating above equation, we obtain a relation among the time tendency of the domain-averaged surface pressure, the mass flux through the lateral boundaries and the total precipitation rate at surface. JMA-NHM dynamically adjusts the mass flux through the lateral boundaries, monitoring the total surface precipitation. In this method, however, magnitude of the adjustment increases with the increase of the model domain. To solve this problem, we evaluate moisture diffusion in the continuity equation as

$$\frac{\partial \rho}{\partial t}+\frac{\partial \rho u}{\partial x}+\frac{\partial \rho v}{\partial y}+\frac{\partial \rho w}{\partial z}=\frac{\partial}{\partial z}(\rho_a V_r q_r+\rho_a V_s q_s+\rho_a V_g q_g)+\rho K\nabla^2 q_v. \qquad (6)$$

Using above equation, the total surface evaporation offsets the total surface precipitation, thus the magnitude of the adjustment for mass flux at lateral boundaries decreases.

References.

Saito, K., 2002: Time-splitting of gravity waves in the Meteorological Research Institute/Numerical Prediction Division unified Nonhydrostatic Model. *CAS/JSC WGNE Research Activities in Atmospheric and Oceanic Modelling*, **32**, 0321-0322.

Saito, K., 2003: Time-splitting of advection in the JMA Nonhydrostatic Model. *CAS/JSC WGNE Research Activities in Atmospheric and Oceanic Modelling*, **33**, 0315-0316.

A change to the physical process of JMA Typhoon Model

Ryota Sakai, Takuya Hosomi
Numerical Prediction Division, Japan Meteorological Agency
1-3-4 Otemachi, Chiyoda-ku, Tokyo 100-8122, JAPAN
E-mail: r-sakai@naps.kishou.go.jp, hosomi@naps.kishou.go.jp

1. Introduction

The Japan Meteorological Agency (JMA) operates the Typhoon Model (TYM) 4 times a day for predicting tropical cyclones in the Western North Pacific. In recent years, TYM has been improved by changing the typhoon bogus system (Sakai et al. 2002), while the JMA Global Spectral Model (GSM) has been improved by changing the physical process as well as data assimilation. Both models have successfully reduced the error on typhoon track forecast. Stimulated by the improvement in GSM, the physical processes of TYM were changed by introducing those implemented in GSM from 1999 to 2001 (Kuma 2001). The major changes are as follows:

(1) Incorporating cloud water content as a prognostic variable (parameterization of precipitation and radiation).

(2) Modifying an Arakawa- Shubert cumulus convection scheme.

(3) In stead of a moist adjustment scheme, introducing a muss-flux type convection scheme for mid-level convection parameterization.

(4) Considering direct effect of aerosols on short-wave radiation.

Some preliminary experiments show, however, that the new TYM often overestimates typhoon intensity. Recent studies report the simulated intensity of a tropical cyclone is sensitive to the ratio of the enthalpy to momentum exchange coefficients, Ck/Cd (Ck: Exchange coefficient for heat and water, Cd: Surface exchange coefficient for momentum). The lower the value of Ck/Cd, the less intense the simulated tropical cyclone (Emanuel 1995; Bao 2003). In order to suppress the overestimation in typhoon intensity forecast, a roughness length on sea surface is changed so that the heat and moisture fluxes on sea surface were decreased (Lower value of Ck/Cd).

(5) The roughness length formulas were changed from Kondo (1975) to Garratt (1992) for the heat and water exchange coefficient and Beljaars (1995) for momentum exchange coefficient.

2. Experiment and Result

Figure 1 shows the track for T0206 (CHATAAN) predicted by the new TYM. Best track and prediction by the old version of TYM as the control run are also indicated. In this forecast period, the typhoon changes its direction from north-westward to north-eastward (re-curvature stage). In the control, the re-curvature is not predicted well and the typhoon continues to move to the north-west. In the case of the new TYM, though the speed of movement is slower than analysis, the re-curvature is predicted well. Figure 2 shows surface pressure and precipitation for 84-hour forecast. In the control, a small low and associated intensive precipitation are predicted in the northeast of the typhoon and the low moves northeastward along the edge of the sub-tropical high. Affected by this small low, the typhoon continues to move northwestward. Actually, the small low nor the intensive precipitation exists around the typhoon. In the new TYM, no spurious low is predicted in the area and the typhoon is predicted well to move along the edge of the sub-tropical high following the anti-cyclonical flow. The new TYM is superior to the control in the prediction of the synoptic field in tropics.

Figure 3 shows the impact of the roughness length formulas to the intensity forecast for T0216 (SINLAKU). Without a change of the roughness length formulas (thin solid line), the predicted central pressure of the typhoon is about 30 hPa stronger than the analysis. By changing the roughness length formulas (broken line), the overestimation is suppressed, and the predicted central pressure is close to the

analysis.

Figure 4 shows the result of the forecast experiment targeting T0206 (CHATAAN), T0216 (SINLAKU) and T0221 (HIGOS). The track-forecast error is reduced by 56km in 72 hour forecast compared to operational one. The intensity-forecast error (Figure 5) is similar to the operational one.

The JMA implemented these changes in operational TYM in July 2003.

Reference

Bao, J- W., S. A. Michelson., J. M. Wilczak, 2002: Sensitivity of numerical simulations to parameterizations of roughness for surface heat fluxes at high winds over the sea. *Mon. Wea. Rev.* **130**, 1926-1932.

Beljaars, A. C. M., 1995: The parameterization of surface fluxes in large-scale models under free convection. *Quart. J. Roy. Meteor. Soc.*, **121**, 255-270.

Emanuel, K. A., 1995: Sensitivity of tropical cyclones to surface exchange coefficients and a revised steady-state model incorporating eye dynamics. *J. Atmos. Sci.*, **52**, 3969-3976.

Garratt, J. R., 1992: The Atmospheric Boundary Layer. Cambridge University Press, 316pp.

Kondo, J., 1975: Air-sea bulk transfer coefficients in diabatic conditions. *Bound. Layer Met.*, **9**, 91-112.

Kuma, K., H. Kitagawa, H. Mino, M. Nagata, 2001: Impact of a recent major version-up of the Global Spectral Model (GSM) at JMA on tropical cyclone predictions. *RSMC Tokyo-Typhoon Center Technical Review,* **No. 4**, 14-20.

Sakai, R. H. Mino, M. Nagata, 2002: Verification s of tropical cyclone predictions of the new numerical models at JMA. *RSMC Tokyo-Typhoon Center Technical Review,* **No. 5**, 1-18.

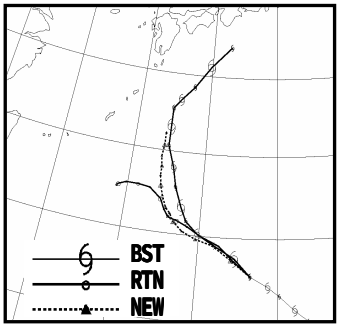

Fig.1 Forecast track for the T0206 (CHATAAN) by TYM (Initial time: 2002/07/06 00 UTC)
BST: Best track, RTN: control, NEW: New TYM. Plotted every 6 hour.

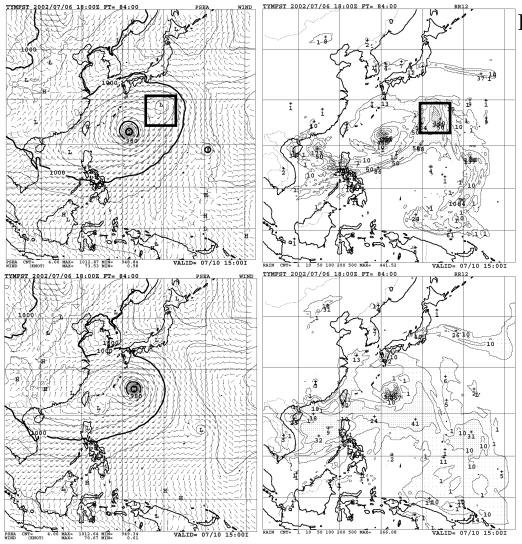

Fig.2 84 hour forecast of the control (upper) and the new (lower) TYM. Mean-sea level pressure (left) and preceding precipitation accumulated 12 hour (right). (Target: T0206 Initial time: 2003/07/06 18UTC)
A spurious low and associated intensive precipitation are indicated with a square.

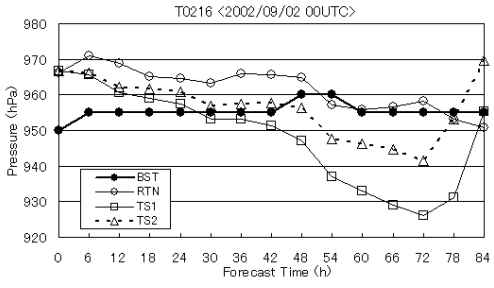

Fig. 3 Intensity forecasts for the T0216 (SINLAKU) by TYM (Initial time: 2002/09/06 00UTC)
BST: Best track, RTN: control, TS1: Without change of the roughness length, TS2: With change of the roughness length.

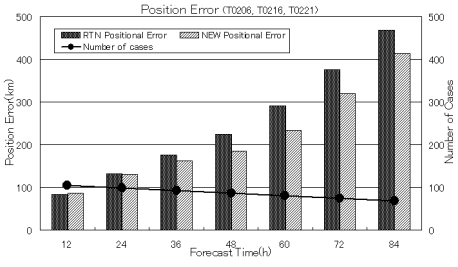

Fig. 4 Mean position error of TYM.
Dark bar is the control. Light bar is the new TYM. Line is the number of cases.

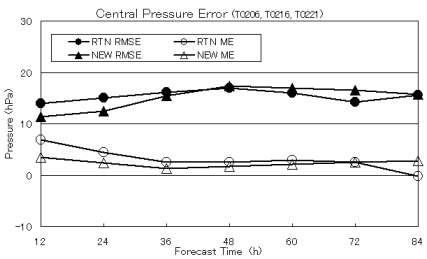

Fig. 5 Central pressure error of TYM.
RTN: control, NEW: new TYM. Closed marker shows root mean square error (RMSE). Open marker shows mean error (ME).

An atmospheric model prediction system for very short range forecasts.

Bent H. Sass and Claus Petersen

Danish Meteorological Institute
(e-mail: bhs@dmi.dk and cp@dmi.dk)

1. The model setup

At the Danish Meteorological Institute (DMI) the atmospheric limited area model DMI-HIRLAM (Sass et al. 2002) is used in a special setup to produce very short range forecasts of cloud cover, precipitation, 2m temperature, dew point and road surface temperture for many ($\approx$ 370) road-weather stations in Denmark. New forecasts are produced hourly and the forecast range is 6 hours. The goal of producing accurate local weather parameters is difficult due to the small scales involved in both space and time.

The model is set up for a limited area around Denmark. Currently the model resolution is 0.15° using 40 model levels in the vertical. The lateral boundary conditions are supplied hourly with time interpotation from the operational model DMI-HIRLAM-E covering a much larger domain. Every time step of the DMI-HIRLAM forecast a special road-weather module (RWM) is called. This module (Sass 1997) completes the special forecasts of the weather parameters mentioned above. The computations involve a local energy budget for a road surface, and site specific features are taken into account. More details about the model setup can be found in Sass and Petersen (2004).

Since the goal is to improve the short range forecast of DMI-HIRLAM the challenge is to assimilate new data which is not already used in the boundary generating model DMI-HIRLAM-E. Currently an assimlation period of 3 hours prior to the forecast initial time is performed. The model is run through this period using a nudging technique (Sass and Petersen 2002a) where the model tendencies of humidity and cloud condensate are modified such that the difference between model predicted and hourly analyses of cloud cover and precipitation is reduced. Close to the surface the DMI-HIRLAM lowest model level temperature and humidity are modified along with the surface temperature and moisture in proportion to the difference between analysed and currently model diagnosed 2m temperature and humidity, respectively. There is a distinction between the size of the nudging coefficient for the lowest model level and the coefficient used for the surface variable, according to their relative importance for the diagnosed parameter at 2m height.

The analysed state used during nudging is determined from a reference forecast (without nudging) combined with synoptic data in an analysis procedure (Sass and Petersen 2002b) using relatively simple weighting procedures for analyses at 2m. The 3-D cloud analysis involves vertical overlap assumptions to utilize synop observations. Recently,

satellite data (SAF based cloud mask from NOAA 16 and 17) has been incorporated in the analysis procedure. The precipitation intensity analysis is at an early stage of development, with many precautions taken.

2. A forecast example

The system described above has been operational since October 2003. However, the use of satellite data is not yet operational. An example showing simulated total cloud cover with and without analysis nudging is shown in Fig.1a (left) and 1b (right), respectively. The result applies to a forecast initial time of 02 UTC on 8 December 2002. The figures confirm that 'nudging' of additional information can lead to important differences in the initial state of the cloud cover. Synoptic observations of total cloud cover during the night on 8 December 2002 (not shown) reveal that the run with cloud assimilation is the most realistic one. Cloud cover differences between the two runs remain throughout a 6-hour forecast, but the differences get smaller later in the prediction. In some cases a positive impact of cloud cover assimilation can be seen beyond a forecast range of 12 hours.

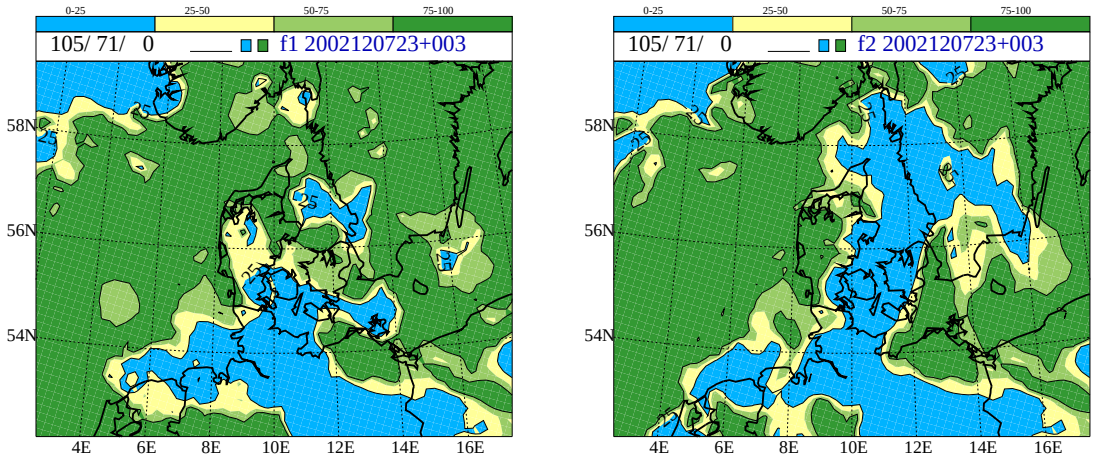

References

Sass, B. (1997). 'A Numerical Forecasting System for the Prediction of Slippery Roads '. J. Appl. Meteor., 36, pages 801-817.

Sass, B. and C. Petersen (2002a). 'Short range atmospheric forecasts using a nudging procedure to combine analyses of cloud and precipitation with a numerical forecast model'. DMI Sci. Rep. no. 02-01, Danish Meteorological Institute.

Sass, B.H. and C. Petersen (2002b). 'Analyses and short range forecasts of cloud cover'. DMI Tech. Rep. no. 02-09, Danish Meteorological Institute.

Sass, B.H., Woetmann, N.W., Jørgensen, J.U., Amstrup, B., Kmit,M. and K.S. Mogensen (2002). 'The operational DMI-HIRLAM system 2002 - version'. DMI Tech. Rep. no. 02-05. Danish Meteorological Institute 2002.

Sass, B.H. and C. Petersen (2004). 'The coupled operational numerical road weather forecasting system at DMI'. DMI Technical Rep. no. 04-01, Danish Meteorological Institute.